To identify the chromosomal transgene integration sites, fluorescence *in situ* hybridization (FISH) was performed. Consistent with the Southern blotting analysis, the FISH results showed several integration sites in the chromosomes of peripheral blood mononuclear cells (MNCs), and further showed that each infant had different transgene integration patterns with patterns the sometimes varied among different MNCs (Supplementary Fig. 1 and Supplementary Data 3). In 584, four transgene integration sites were seen, on chromosomes 2, 7 and 13; in 587, two distinct signals were recognized in the peripheral blood lymphocyte DNA, on chromosomes 3 and 12. No signal was detected in the peripheral blood lymphocyte samples from 588, and several transgene integration patterns were seen in 594 and 666. Infant 594 had at least three different transgene integration patterns, and more than six patterns may have occurred. Infant 666 showed the largest number of integration patterns, up to 13. Moreover, although this animal was male, of the 13 investigated karyograms, eight samples were of the female karyotype, owing to haematopoietic chimaerism caused by blood exchange with his twin, 594.

Expression of the EGFP transgene

EGFP messenger RNA was detected in the hair roots of all the infants except 588 and in the peripheral blood cells of 584 and 587, by RT–PCR. Transcription of the EGFP gene was indicated in all of the placental samples, 584, 588 and 594/666 (Fig. 3a–c).

To assess EGFP expression in tissues, EGFP fluorescence was examined directly by fluorescence microscopy, and immunohistochemical analysis of the hair roots, frozen sections of a small piece of ear tissue, and placenta samples was performed (Fig. 3d–g). EGFP was strongly expressed in the epidermal cells of the ear tissue and stromal cells of the placenta. In all of the animals except 588, EGFP expression was observed in the hair roots and skin. Placental samples from 584 and 588 also showed high levels of EGFP, but it was undetectable in 594/666 (Supplementary Figs 2–4).

Peripheral blood samples were subjected to flow cytometric analysis using a FACScant. FACS analysis showed EGFP-positive peripheral blood MNCs in 584 and 587. The proportion of EGFP-positive cells was 15.7 and 19.1%, respectively (Fig. 3h). The flow cytometry results corresponded well with those from RT–PCR. Among the peripheral blood cells, the EGFP-positive percentage of granulocytes, lymphocytes and monocytes was 34.5, 3.3 and 18.0% in 584, and 47.7, 4.6 and 20.0% in 587, respectively (Supplementary Fig. 5).

Germline transmission of the transgene

At the moment when two of the animals (666 and 584) became sexually mature, the transgene expression in their gametes was analysed. Semen samples were collected from 666, and live spermatozoa were obtained by the swim-up method in TYH medium. RT–PCR analysis demonstrated the presence and expression of the transgene in the germ cells of 666 (Fig. 4a). IVFs were then performed using semen collected from 666 and wild-type oocytes to analyse the fertility of the germ cells carrying the transgene. Fluorescence microscopy showed that 20–25% of the IVF embryos strongly expressed EGFP, as shown in Fig. 4b. Furthermore, three pre-implantation live natural embryos were collected from female animal 584, and one of these embryos strongly expressed EGFP. The IVF embryos from 666 and two of the natural blastocyst embryos from 584 were shown to express the EGFP transgene by RT–PCR (Fig. 4a). Three EGFP-positive IVF embryos from the male animal (666) were then transferred into a surrogate mother. One neonate (687) was delivered at full term by caesarean section, and this neonate carried the EGFP gene and expressed the transgene in skin (Fig. 4c–e), but not in the placenta and hair.

Discussion

To our knowledge, this is the first report of transgenic non-human primates showing not only the transgene expression in somatic tissues, but also germline transmission of the transgene with the full, normal

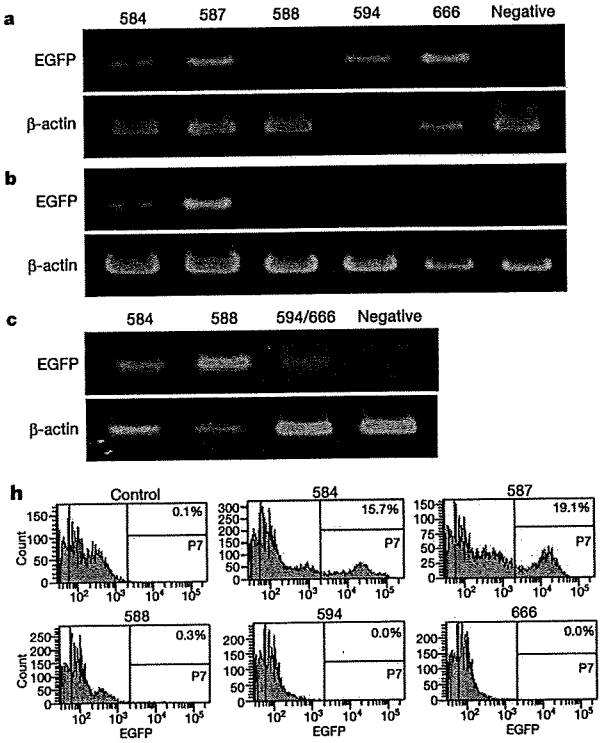

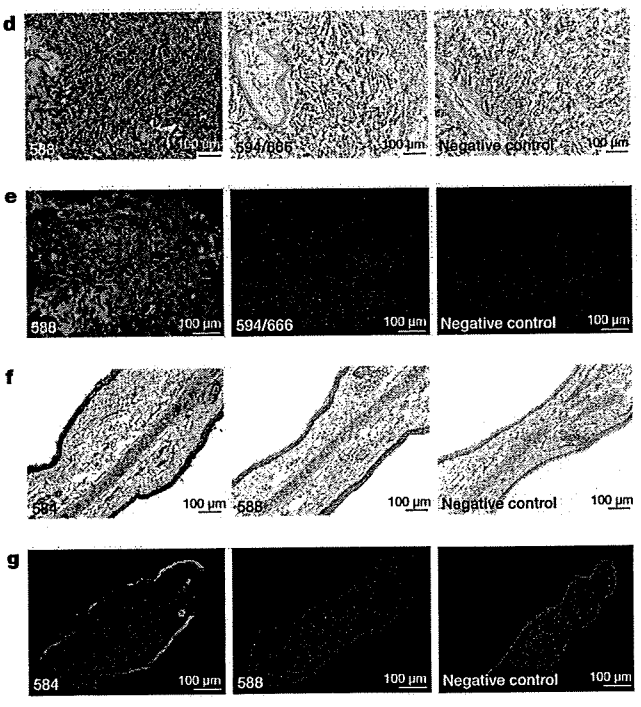

Figure 3 | Transgene transcription and expression in several infant tissues. **a–c**, RT–PCR results from hair roots (**a**), peripheral blood (**b**) and placenta (**c**). Each lane indicates the animal number. **d–g**, Immunohistochemical (**d**, **f**) and epifluorescence (**e**, **g**) analyses using an anti-EGFP antibody, of frozen ear tissues (**f**, **g**) and placentae (**d**, **e**). Scale bars, 100 μm. **h**, Results of FACS analysis using whole peripheral blood cells. The percentage of EGFP-positive cells is shown in the top right of each panel.

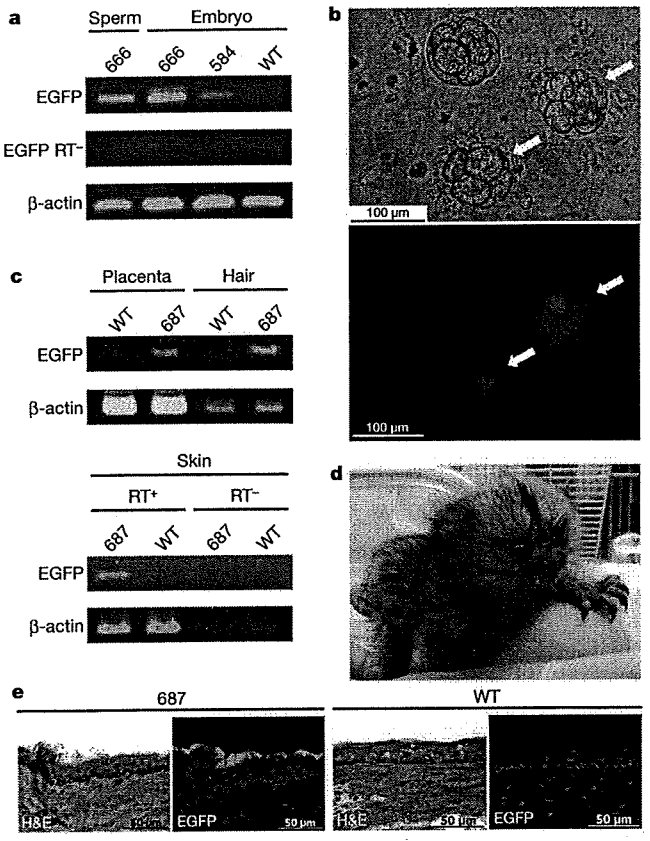

Figure 4 | Germline transmission of the transgene. **a**, RT–PCR analysis of spermatozoa and IVF embryos from 666, and natural embryos from 584. RT− denotes the absence of reverse transcriptase as a control. **b**, Bright-field and dark-field of epifluorescence images of IVF embryos. EGFP-positive IVF embryos produced with 666 spermatozoa are indicated by white arrows. **c**, PCR (top panel) and RT–PCR (bottom panel) analysis of the tissues from the F_1 neonate. **d**, Photograph of the F_1 offspring (687) from 666. **e**, Haematoxylin and eosin (H&E) staining and epifluorescence imaging of frozen skin tissue from the neonate. WT, wild-type control.

development of the embryo. We obtained five transgenic marmosets, four of which expressed the transgene in several somatic cell lineages, such as hair root, skin fibroblast and peripheral blood cells. The remaining animal expressed the transgene only in the placenta. Two of these animals reached sexual maturity and showed the transgene insertion and expression in germ cells. Epifluorescence microscopic observation and RT–PCR analysis of embryos generated by transgene-bearing gametes strongly indicated that the transgenic germ cells from animals 666 and 584 were fertile, and this was proved for the male (666) who fathered one healthy, transgenic infant (687) with the transgene expression in the somatic cells. These findings suggest that it should be possible to establish transgenic non-human primate colonies, opening the door to their use in biomedical research.

Because the manipulation of embryos for viral injection and their subsequent culture may affect embryonic development, the birth rate after embryo transfer (6.25%) was lower than that for normal embryos (30.7%, data not shown). The miscarriage rates were not significantly different between embryonic transfers performed using normal embryos (28.6%) and transgenic embryos (42.6%). Despite considerable effort, transgenic marmosets have not been produced by DNA pronuclear microinjection. The production rate that we obtained using lentivirus (5.26–6.25%) suggests that our technique is sufficiently effective for the production and use of genetically modified marmosets as human disease models.

The 100% birth rate of transgenic marmosets achieved in the present study could be due to several technical advantages. First, we used EGFP as the transgene, enabling us to monitor the presence and expression of the transgene at each experimental step in live embryos and the transgenic animals. Accordingly, we were able to select unambiguously EGFP-expressing embryos for transfer into surrogate mothers. This selection was effective, not only for increasing the birth rate of transgenic animals, but also for reducing the number of surrogate mother animals needed.

Second, we used pre-implantation embryos obtained by natural intercourse, high-titre lentiviral vectors, and 0.25 M sucrose solution as a medium for injection. Even though the birth rates (birth per embryonic transfer) were no different between IVF and natural embryos, the fertilization rate of the germinal vesicle-stage oocytes was quite low. Because it is difficult to collect large quantities of oocytes, it was advantageous to use marmoset natural embryos. To inject as much lentiviral vector as possible into the perivitelline space, the embryos were placed in 0.25 M sucrose medium at the time of lentiviral vector injection, which expanded the volume of the perivitelline space 1.2–7.5-fold. For example, the estimated volume of the perivitelline space of one marmoset pronuclear stage embryo was approximately 31.5 pl, but when placed in 0.25 M sucrose medium, it expanded to about 231 pl. A high titre of the lentiviral vector solution was used so that many lentiviral vector particles were injected into the expanded perivitelline space; approximately 1.3×10^3–1.3×10^5 transducing units of lentiviral vector were injected in this study. Each of these steps probably contributed to the successful production of transgenic marmosets.

The high number of injected lentiviral vector particles resulted in several transgene integrations, as observed by Southern blot analysis and FISH. The embryos injected with the transgene before the four-cell stage (584 and 587) showed fewer than four copies of the transgene per genome by Southern blotting and FISH. The three other embryos (588, 594 and 666), which received the injection at the morula stage, exhibited several integrations of the transgene by Southern blotting and FISH. As the FISH analysis was performed using only peripheral blood MNCs, other patterns of transgene integration cells may have existed in other tissues. The FISH results for 666 were consistent with this hypothesis, as the integration sites in the chimaeric blood MNCs from his twin, 594, were different from those in the blood MNCs of 594.

The lentiviral vector used in the present study can be used to transmit only relatively small transgenes, 8.5 kilobases of DNA or less. Therefore, further study will be necessary to enable the introduction of larger transgenes into marmoset embryos. Furthermore, to study human diseases involving the malfunctions of specific genes, targeted gene-knockdown marmosets could be developed using RNA interference (RNAi) lentiviruses.

The results of the present study indicate that transgenic marmosets may be used as experimental animals for biomedical research. Recently, somatic cell nuclear-transferred embryonic stem cells from the rhesus macaque and induced pluripotent stem cells from adult human fibroblasts were reportedly established[12–15]. Those studies indicated that the obstacle caused by immunogenetic incompatibility has at least theoretically been resolved, and that a new era of regenerative medicine using somatic cell nuclear-transferred embryonic stem cells in primates[14] or human induced pluripotent stem cells[12,13,15] has become possible. However, before such stem cells can be used in clinical applications, preclinical assessments of their safety and efficacy are essential. We previously reported that marmosets with injured spinal cords can recover motor function after the transplantation of human neural stem/progenitor cells[16], highlighting the usefulness of the marmoset for assessing the safety and efficacy of, not only these cells, but also of other stem cells, such as human embryonic stem cells[17] or induced pluripotent stem cells. Human disease models in non-human primates have so far been limited to mechanical injury models (for example, spinal cord injury[18]) and drug administration models (for example, MPTP-induced Parkinson's[19,20]). The only transgene-induced primate disease model is of Huntington's disease[7], in rhesus

monkeys expressing a mutant human huntingtin gene. In that report, although the transgene was inserted into the genome of founder infants and its expression was detected in post-mortem animals, the germline transmission of the transgene has not yet been confirmed[7]. Thus, at this point, it is not certain how reproducible the effects of various therapeutic interventions would be using a large number of animals.

The technique by which we achieved transgene expression in several tissues, along with germline transmission, may provide the means to obtain genetically modified non-human primate models for translational research, investigations of regenerative medicine and gene therapy, and clarification of the scientific gaps among transgenic mice, human disease models, and real human diseases.

METHODS SUMMARY

All animal experiments were approved by the institutional animal care and use committee, and were performed in accordance with Central Institution for Experimental Animal (CIEA) guidelines.

To obtain oocytes, recombinant human follicle stimulating hormone (r-hFSH; 50 international units (IU); Fertinome, Serono) was administered daily by intramuscular injection for 11 days. Human chorionic gonadotropin (hCG; 75 IU; Gonatropin, Teikoku-zouki) was administered by intramuscular injection at 17:30 on day 12. On day 13, the animals were anaesthetized and follicular aspiration was performed surgically. Oocytes were incubated for 24 h at 38 °C, 5% CO_2 in air, for *in vitro* maturation. After incubation, only matured oocytes (metaphase II) were collected and used for IVF.

Ejaculated semen was collected in TYH medium (Mitsubishi Kagaku Iatron), using a Ferti Care personal vibrator. Hyaluronidase-treated oocytes were placed in 70-μl drops of TYH, and an aliquot of sperm (4×10^5) was added to each oocyte incubation drop. After 26–30 h of insemination, the fertilized oocytes were placed into ISM1 (Medicult) medium, and lentiviral vector injection was performed in 0.25 M sucrose.

Natural embryo collection was performed as previously described[21]. Embryos at the pronuclear-to-morula stage were placed in 0.25 M sucrose supplemented PB1 medium (Mitsubishi Chemical Medience Corporation) and injected with lentiviral vector. Blastocysts were not treated with sucrose. Lentiviral vector injection was performed using an Eppendorf FemtoJet express and a Narishige micromanipulator. The embryos were cultured until GFP expression was confirmed.

The ovulation cycles of donor and recipient animals were synchronized, and EGFP-expressing embryos were transferred as previously described[22,23]. After embryo transfer, the recipients were tested for pregnancy by plasma progesterone once a week. The resulting infants were analysed for transgene integration, transcription and expression, by real-time PCR, Southern blot analysis, RT–PCR, immunohistochemical analysis, FACS and FISH.

Full Methods and any associated references are available in the online version of the paper at www.nature.com/nature.

Received 27 September 2008; accepted 30 April 2009.

1. Mansfield, K. Marmoset models commonly used in biomedical research. *Comp. Med.* 53, 383–392 (2003).
2. Chan, A. W., Homan, E. J., Ballou, L. U., Burns, J. C. & Bremel, R. D. Transgenic cattle produced by reverse-transcribed gene transfer in oocytes. *Proc. Natl Acad. Sci. USA* 95, 14028–14033 (1998).
3. Hofmann, A. *et al.* Efficient transgenesis in farm animals by lentiviral vectors. *EMBO Rep.* 4, 1054–1060 (2003).
4. Hofmann, A. *et al.* Generation of transgenic cattle by lentiviral gene transfer into oocytes. *Biol. Reprod.* 71, 405–409 (2004).
5. Chan, A. W., Chong, K. Y., Martinovich, C., Simerly, C. & Schatten, G. Transgenic monkeys produced by retroviral gene transfer into mature oocytes. *Science* 291, 309–312 (2001).
6. Wolfgang, M. J. *et al.* Rhesus monkey placental transgene expression after lentiviral gene transfer into preimplantation embryos. *Proc. Natl Acad. Sci. USA* 98, 10728–10732 (2001).
7. Yang, S. H. *et al.* Towards a transgenic model of Huntington's disease in a non-human primate. *Nature* 453, 921–924 (2008).
8. Rogers, C. S. *et al.* Disruption of the *CFTR* gene produces a model of cystic fibrosis in newborn pigs. *Science* 321, 1837–1841 (2008).
9. Rogers, C. S. *et al.* Production of *CFTR*-null and *CFTR-ΔF508* heterozygous pigs by adeno-associated virus-mediated gene targeting and somatic cell nuclear transfer. *J. Clin. Invest.* 118, 1571–1577 (2008).
10. Miyoshi, H., Blomer, U., Takahashi, M., Gage, F. H. & Verma, I. M. Development of a self-inactivating lentivirus vector. *J. Virol.* 72, 8150–8157 (1998).
11. Ross, C. N., French, J. A. & Orti, G. Germ-line chimerism and paternal care in marmosets (*Callithrix kuhlii*). *Proc. Natl Acad. Sci. USA* 104, 6278–6282 (2007).
12. Takahashi, K. *et al.* Induction of pluripotent stem cells from adult human fibroblasts by defined factors. *Cell* 131, 861–872 (2007).
13. Yu, J. *et al.* Induced pluripotent stem cell lines derived from human somatic cells. *Science* 318, 1917–1920 (2007).
14. Byrne, J. A. *et al.* Producing primate embryonic stem cells by somatic cell nuclear transfer. *Nature* 450, 497–502 (2007).
15. Nakagawa, M. *et al.* Generation of induced pluripotent stem cells without Myc from mouse and human fibroblasts. *Nature Biotechnol.* 26, 101–106 (2008).
16. Iwanami, A. *et al.* Transplantation of human neural stem cells for spinal cord injury in primates. *J. Neurosci. Res.* 80, 182–190 (2005).
17. Thomson, J. A. *et al.* Embryonic stem cell lines derived from human blastocysts. *Science* 282, 1145–1147 (1998).
18. Iwanami, A. *et al.* Establishment of graded spinal cord injury model in a nonhuman primate: the common marmoset. *J. Neurosci. Res.* 80, 172–181 (2005).
19. Eslamboli, A. Marmoset monkey models of Parkinson's disease: which model, when and why? *Brain Res. Bull.* 68, 140–149 (2005).
20. Ando, K. *et al.* Neurobehavioral protection by single dose l-deprenyl against MPTP-induced parkinsonism in common marmosets. *Psychopharmacology (Berl.)* 195, 509–516 (2008).
21. Sasaki, E. *et al.* Establishment of novel embryonic stem cell lines derived from the common marmoset (*Callithrix jacchus*). *Stem Cells* 23, 1304–1313 (2005).
22. Lopata, A., Summers, P. M. & Hearn, J. P. Births following the transfer of cultured embryos obtained by *in vitro* and *in vivo* fertilization in the marmoset monkey (*Callithrix jacchus*). *Fertil. Steril.* 50, 503–509 (1988).
23. Summers, P. M., Shephard, A. M., Taylor, C. T. & Hearn, J. P. The effects of cryopreservation and transfer on embryonic development in the common marmoset monkey, *Callithrix jacchus*. *J. Reprod. Fertil.* 79, 241–250 (1987).

Supplementary Information is linked to the online version of the paper at www.nature.com/nature.

Acknowledgements We thank F. Toyoda, S. Ohba, T. Inoue, Y. Sawada and M. Yokoyama for technical assistance with the animal experiments and care. E.S. is an associate professor of the Global COE program for human metabolomic systems biology assigned to Keio University. This study was also supported by the Global COE program for Education and Research Centre for Stem Cell Medicine from the Ministry of Education, Culture, Sports, Science and Technology (MEXT), the Japanese Government to Keio University. This study was also supported by funds from Solution-Oriented Research for Science and Technology (SORST) of the Japan Science and Technology Agency and grants from MEXT to H.O. and from Special Coordination Funds for Promoting Science and Technology of MEXT to S.H.

Author Contributions E.S. designed the experiments, conducted the project, and wrote the paper. A.S., Y.S., T.E., I.T. and R.H. assisted in embryological technique development. K.H., R.O. and M.K. developed surgical techniques for embryo collection and transfer. H.S., C.K. and C.Y. performed or assisted with the real-time PCR and parentage evaluation test. S.S. and T.M. assisted with the Southern blot analysis and tissue collection. M.I. raised the anti-marmoset CD45 antibody. R.I. performed the FACS analysis, and K.K. performed the immunohistochemical analysis. H.M. provided the lentiviral vectors. Y.T., H.O., S.H., N.T. and T.N. designed the project, and H.O., S.H. and N.T. also participated in writing the paper. The whole project was supervised by E.S. and H.O.

Author Information Reprints and permissions information is available at www.nature.com/reprints. Correspondence and requests for materials should be addressed to E.S. (esasaki@ciea.or.jp) or H.O. (hidokano@sc.itc.keio.ac.jp).

METHODS

Animals. Adult common marmosets more than 2 years old were obtained from a marmoset breeding colony for experimental animals. Female marmosets with normal ovarian cycles were paired with intact males for natural embryo collection. Recipient females were paired with vasectomised males or intact females. This study was approved by the Institutional Animal Care and Use Committee of CIEA, and was performed in accordance with CIEA guidelines.

***In vitro* fertilization.** Semen was collected as previously described for common marmosets[24]. Ejaculated semen was collected in TYH medium (Mitsubishi Kagaku Iatron) and washed twice with TYH. The semen was placed in a CO_2 incubator for 10 min in a test tube inclined at a 30° angle to allow the sperm to swim up. Hyaluronidase-treated metaphase-II-arrested oocytes were inseminated with a final concentration of 5×10^6 sperm ml^{-1} for 26–30 h. Fertilized embryos were cultured in ISM medium (Medicult, Nosan Corp.).

Embryo collection and transfer. Embryo collection and transfer were performed as previously described[25]. After embryo transfer, the recipients were monitored for pregnancy by measuring their plasma progesterone once a week until the pregnancies could be monitored by transabdominal palpation of the uterus.

Lentiviral vector preparation and transduction. The lentiviral vectors were produced as previously described[26]. The medium containing viral particles was spun at 4 °C, 50,000*g* for 4 h, and the viral pellet was then resuspended in ISM2 medium, in 1/1,000 of the volume of the original lentiviral vector supernatant. To measure the lentivirus titre, serially diluted (10^{-2} to 10^{-8}) lentiviral vector was used to infect 10^5 293T cells. The number of EGFP-positive cells was counted by FACS to quantify the titre.

Pronuclear-to-morula stage embryos were placed in 0.25 M sucrose supplemented PB1 medium (Mitsubishi Chemical Medience Corporation), and the virus was injected into the perivitelline space. For blastocyst embryos, the viral vector was injected into the blastocoel. All viral injections were performed using an Eppendorf FemtoJet Express and a Narishige micromanipulator.

Southern blot analysis. Five micrograms of genomic DNA was digested with BamHI for animals that had been injected with CAG-EGFP, and with EcoRI for those that had been injected with CMV-EGFP. The digested genomic DNA was separated on a 0.8% agarose gel and transferred to a Hybond-N+ nylon membrane (GE Healthcare Biosciences). Southern blot analysis was performed using the DIG system (Roche Diagnostics K.K.), according to the manufacturer's protocol. CMV-EGFP was digested with EcoRI and then labelled with DIG using the PCR DIG probe synthesis kit, according to the manufacturer's instructions (Roche Diagnostics K.K.).

RT–PCR. To detect EGFP gene expression, EGFP5-5 (5′-GCACAAGCTGGAGT ACAACTACAACAGC-3′) and EGFP3-1 (5′-TCACGAACTCCAGCAGGACC AT-3′) primers were used. To detect β-actin expression, β-actin 001 (5′-TCCTG ACCCTGAAGTACCCC-3′) and β-actin 002 (5′-GTGGTGGTGAAGCTGTA GCC-3′) primers were used. PCR was performed for 35 cycles of denaturation at 94 °C for 30 s, annealing for 30 s at 58 °C for EGFP primers or 62 °C for β-actin primers, and elongation at 72 °C for 30 s.

To detect EGFP gene expression in germ cells and neonatal tissues, PCR was performed using the EGFP5-4 (5′-CAAGGACGACGGCAACTACAAGACC-3′) and EGFP3-3es (5′- GCTCGTCCATGCCGAGAGTGA-3′) primers. Then, 1 μl of the PCR products was re-amplified with the EGFP5-6 (5′-TCGAGCTGA AGGGCATCGAC-3′) and EGFP3-1 (5′-TCACGAACTCCAGCAGGACCAT-3′) primers. To detect β-actin expression, the PCR primers β-actin 003 (5′-TGGACTTCGAGCAGGAGAT-3′) and β-actin 006R (5′-CCTGCTTGCTG ATCCACATG-3′) were used. Then, 0.5 μl of the PCR products was re-amplified with the 004 (5′-TCCCTGGAGAAGAGCTATG-3′) and 005R (5′-GAGC CACCAATCCACACTGA-3′) primers. PCR was performed for 30 cycles of denaturation at 98 °C for 10 s, annealing at 60 °C for 10 s, and elongation at 72 °C for 30 s.

Immunohistochemical analysis. Tissues were embedded in OCT compound, frozen in liquid nitrogen, and sliced into 5-μm sections, which were fixed in 4% paraformaldehyde for 30 min at 4 °C. Endogenous peroxidase activity was quenched using 0.03% hydrogen peroxidase for 30 min at room temperature. The slides were blocked with 10% goat serum (Nichirei) for 10 min at room temperature and then reacted with the rabbit anti-GFP polyclonal antibody (A.v. peptide antibody, BD Bioscience) overnight at 4 °C. The slides were incubated with the biotinylated secondary antibody Simple Stain Mouse MAX PO (Nichirei) for 30 min at room temperature. The bound antibodies were detected with DAB (3,3-diaminobenzidine tetrahydrochloride) horseradish peroxidase complex. The samples were then stained with H&E and examined by microscopy.

FACS analysis. Whole blood cells were washed with PBS and suspended in 0.13 M NH_4Cl. The pellet was incubated with the mouse IgG1 anti-marmoset CD45, 6C9 antibody for 30 min on ice[27], then mixed with an allophycocyanin (APC)-labelled anti-mouse IgG antibody, and incubated for 30 min on ice. The sample was washed with PBS and resuspended in 200 μl of propidium iodide solution. FACScant analysis was then performed.

Fluorescent *in situ* hybridization. Peripheral blood samples were cultured in RPMI 1640 containing phytohaemagglutinin, concanavalin A, lipopolysaccharide, and 2-mercaptoethanol for 2–3 days. After 2–3 h of incubation with BrdU (final concentration 30 μg ml^{-1}), colcemid (final concentration 0.02 μg ml^{-1}) was added to the medium, and the samples were incubated for another 2 h. After lymphocyte fixation, the cells were spread on slides and air-dried overnight, then stained with Hoechst 33258 and treated with ultraviolet light. CAG-EGFP was labelled with digoxigenin-11-dUTP as a probe, and hybridized at 37 °C overnight. After stringent washes, the bound label was detected using anti-Dig-Cy3. For karyotyping, Leica CW4000 FISH and Leica CW4000 Karyo were used.

24. Kuederling, I., Schneiders, A., Sonksen, J., Nayudu, P. L. & Hodges, J. K. Non-invasive collection of ejaculates from the common marmoset (*Callithrix jacchus*) using penile vibrostimulation. *Am. J. Primatol.* 52, 149–154 (2000).
25. Summers, P. M., Shephard, A. M., Taylor, C. T. & Hearn, J. P. The effects of cryopreservation and transfer on embryonic development in the common marmoset monkey, *Callithrix jacchus*. *J. Reprod. Fertil.* 79, 241–250 (1987).
26. Bai, Y. *et al.* Effective transduction and stable transgene expression in human blood cells by a third-generation lentiviral vector. *Gene Ther.* 10, 1446–1457 (2003).
27. Ito, R. *et al.* Novel monoclonal antibodies recognizing different subsets of lymphocytes from the common marmoset (*Callithrix jacchus*). *Immunol. Lett.* 121, 116–122 (2008).

CD73, a Novel Cell Surface Antigen That Characterizes Retinal Photoreceptor Precursor Cells

Hideto Koso,[1] *Chiharu Minami,*[1,2] *Yoko Tabata,*[1] *Mariko Inoue,*[1] *Erika Sasaki,*[3] *Shinya Satoh,*[1] *and Sumiko Watanabe*[1]

Purpose. The authors sought to identify cell surface markers of photoreceptor and its precursor cells.

Methods. The expression of surface CD antigens that label both temporally and spatially distinct populations of mouse retinal cells were examined. Of the antibodies that showed positive signals in retinal cells, CD73 was focused on for more detailed analyses.

Results. Mouse retinal subpopulations that expressed CD73 first appeared around birth and subsequently increased dramatically in number, eventually representing more than 90% of the retinal cells in the adult. $CD73^+$ cells were postmitotic and mostly rhodopsin-negative at postnatal day 1. However, in the adult retina, most of these cells expressed rhodopsin but not s-opsin. In reaggregation cultures, $CD73^+$ cells differentiated into rhodopsin-positive cells more rapidly than $CD73^-$ cells, which supports the idea that CD73 is an early photoreceptor lineage marker. The effects of ectopic expression in retinal cells of Nrl and Crx, both of which are transcription factors known to be expressed in photoreceptor lineage, suggest that CD73 is genetically downstream of Crx in the rod cell differentiation lineage. Adult retina of the common marmoset monkey also showed correlation of the expression pattern of rhodopsin and CD73.

Conclusions. CD73 is a cell surface marker of cone/rod common precursors and mature rod cells in mice and is genetically localized between Nrl and Crx. The expression of CD73 was conserved in primate rod cells, and CD73 provides an useful tool to purify photoreceptor cells for transplantation aimed at the regeneration of photoreceptors. (*Invest Ophthalmol Vis Sci.* 2009;50:5411–5418) DOI:10.1167/iovs.08-3246

The vertebrate neural retina consists of six types of neurons and one type of glial cells, which are organized into a laminar structure. The outer nuclear layer (ONL) consists of photoreceptors, and specific loss of these cells causes several severe retinal diseases, among them retinitis pigmentosa.[1,2] Regeneration of photoreceptor cells is an important step in the regeneration of vision, and considerable effort is being invested in understanding these processes. The isolation of retinal progenitor cells or precursors of the photoreceptors lineage is one of the strategies used to achieve neural retina regeneration by transplantation.[3] However, these cell populations have not yet been adequately characterized, in part because of a lack of markers that can be used to identify the distinct stages and lineages of retinal cells. Although the patterns of expression of transcriptional factors reported to be involved in retinal development may reflect the developmental stage, these molecules are intracellular, which limits their usefulness for cell enrichment. Therefore, it is important to define surface markers that can be used to label specific retinal cell subpopulations. Surface antigens permit the isolation of a specific subset of cells from a cell mixture without damaging the cells, which facilitates the characterization of cell lineages and the identification of factors that regulate cell proliferation and differentiation. We evaluated candidate markers using flow cytometry and cell sorting in combination with retinal in vitro cultures. We screened the mouse retina at various developmental stages for reactivities with a panel of antibodies directed against cell-surface antigens and obtained unique expression patterns for more than 30 antigens. Among these, SSEA-1 (CD15) and c-kit (CD117) have been shown previously to represent the early and late immature stages of retinal progenitor cells, respectively.[4,5]

In the present study, we focused on the CD73 antigen, the expression of which was seen to increase concomitantly with retinal development. CD73, which is also known as ecto-5′-nucleotidase, is a 70-kDa glycosylphosphatidylinositol (GPI)-anchored cell surface molecule that catalyzes the extracellular conversion of 5′-adenosine monophosphate to adenosine.[6,7] We identified CD73 as a marker of the early stages of the photoreceptor lineage. CD73 is assumed to be localized genetically downstream of Crx. This is the first report describing a cell surface marker of immature photoreceptor cells.

Materials and Methods

Mice, Common Marmoset, and Cultures

EGFP transgenic mice, which were kindly provided by Masaru Okabe (Osaka University, Japan),[8,9] were maintained in a C57BL/6J background. ICR mice were obtained from Japan SLC. Common marmoset was maintained in the Central Institute for Experimental Animals (CIEA) in accordance with CIEA guidelines. Retinal explant cultures and reaggregation cultures were prepared as described previously[4,10] and were infected with retroviruses as described previously.[10,11] All animal experiments were approved by the Animal Care Committee of the Institute of Medical Science, University of Tokyo and adhered to the ARVO Statement for the Use of Animals in Ophthalmic and Vision Research.

Fluorescence-Activated Cell Sorting

Neural retinas were isolated and dispersed to single cells using trypsin and were stained with antibodies, as described previously.[4] The following antibodies were used: anti-CD73 (BD Bioscience, Franklin Lakes, NJ), anti-Ki67 (BD Biosciences), anti-Rho4D2 (kind gift from

From the [1]Department of Molecular and Developmental Biology, Institute of Medical Science, University of Tokyo, Tokyo, Japan; the [2]Tokyo College of Biotechnology, Tokyo, Japan; and the [3]Central Institute for Experimental Animals, Kawasaki, Kanagawa, Japan.

Supported by a grant-in-aid from the Ministry of Education, Culture, Sports, Science, and Technology of Japan.

Submitted for publication December 2, 2008; revised April 12, 2009; accepted August 7, 2009.

Disclosure: **H. Koso**, None; **C. Minami**, None; **Y. Tabata**, None; **M. Inoue**, None; **E. Sasaki**, None; **S. Satoh**, None; **S. Watanabe**, None

The publication costs of this article were defrayed in part by page charge payment. This article must therefore be marked "*advertisement*" in accordance with 18 U.S.C. §1734 solely to indicate this fact.

Corresponding author: Sumiko Watanabe, Department of Molecular and Developmental Biology, Institute of Medical Science, University of Tokyo, 4-6-1 Shirokanedai, Minato-ku, Tokyo 108-8639, Japan; sumiko@ims.u-tokyo.ac.jp.

Robert Molday, University of British Columbia, Canada), anti-Nestin (BD Biosciences), anti-PNR (Perseus Proteomics, Tokyo, Japan), and anti-protein kinase C (anti-PKC; Oncogene Research Products, San Diego, CA). Nonlabeled antibodies were visualized with the appropriate secondary antibody conjugated with Alexa488 (Molecular Probes, Eugene, OR). At least 10,000 events for healthy cells were analyzed (FACSCalibur; BD Biosciences). Cell sorting was carried out (FACSVantage or FACSAria; BD Biosciences), as described previously,[4] and results (FACSAria; BD Biosciences) were replotted (FlowJo software; Tree Star, Ashland, OR)

Construction and Immunostaining

The full-length cDNAs of the mouse *Crx*, *Nrl*, and *CD73* genes were cloned by polymerase chain reaction (PCR) according to the sequences in the database using mouse retinal cDNA. The PCR products were cloned into a vector (pGEM-T-Easy; Promega, Madison, WI), and the inserts were subcloned into the pMX-IRES-EGFP retrovirus vector.[10] Immunostaining for sectioned or dissociated retinas was performed as described previously.[4,10] The primary antibodies used were anti-CD73, anti-rhodopsin (Rho4D2), anti-s-opsin (Chemicon, Temecula, CA), anti-glutamine synthetase (Chemicon), and anti-m-opsin (Chemicon). The primary antibodies were visualized using the appropriate secondary antibodies conjugated to Alexa-488 or Alexa-546 (Molecular Probes). DAPI was used for nuclear staining. Samples were mounted (Vecta-Shield; Vector Laboratories, Burlingame, CA) and analyzed under a microscope (Axioplan; Zeiss, Thornwood, NY).

RT-PCR

Total RNA was purified from $CD73^+$ and $CD73^-$ retinal cells using the reagent (TRIZOL; Gibco BRL, Grand Island, NY), and cDNA was synthesized by reverse transcriptase (Superscript II; Gibco BRL). All the primer sets were tested for different numbers of cycles (25–35 cycles) using rTaq (Takara, Shiga, Japan), and the semiquantitative cycle number was determined for each primer set. DNA bands were visualized with ethidium bromide.

Results

Characterization of $CD73^+$ Cells in the Developing Retina

By screening the expression patterns of various CD antigens in the mouse retina at various developmental stages, we noted that the expression levels of some antigens changed as retinal development progressed. The expression of the CD73 antigen increased dramatically with retinal development. Initially, we examined CD73 expression in the mouse neural retina at various developmental stages using flow cytometry (Fig. 1A). CD73 expression was not detected in the retina at embryonic day (E) 14 and was first observed in approximately 10% of the cells derived from an E16 mouse (Fig. 1A). The population of CD73-expressing cells increased along with mouse development until postnatal day (P) 6, and 90% of the cells in the adult mouse retina expressed CD73.

Double immunostaining of CD73 and Ki67, which is a nuclear cell proliferation-associated antigen,[12] showed that CD73 expression in postmitotic cells (Fig. 1B). However, between 10% and 20% of $CD73^+$ cells are Ki67/CD73 double positive at P1 and E17 (data not shown), suggesting that retinal progenitor cells begin to express CD73 at the end of their proliferative stage. We also examined whether $CD73^+$ cells had the characteristics of differentiated lineages of the retinal subpopulation by costaining. Nestin is expressed in neural progenitor cells.[13] None of $CD73^+$ cells coexpressed nestin at P9, which confirms that the $CD73^+$ cell fraction is enriched for differentiated cells. PKC, which is a marker of bipolar cells, was expressed only in a negligible fraction (3%) of the $CD73^{low}$ cells at P9 (Fig. 1C). Similar results were obtained by staining adult retinal cells with antibodies against CD73 and PKC or Islet-1, which are markers of bipolar or amacrine cells, respectively (Fig. 1D). In addition to these results, our immunostaining data do not support the idea that CD73 is expressed in retinal cells other than rod photoreceptors. However, our observation that 85% to 90% of the adult retinal cells were $CD73^+$ by FACS analysis is higher than the generally accepted value for rod photoreceptors (70%). One possible explanation for this discrepancy is the selective loss of retinal cells other than rod photoreceptors during the preparation of single cells by dissociation for FACS analysis.

Rod photoreceptor cells express rhodopsin and represent the largest of the retinal cell subpopulations; these cells differentiate during the last stage of retinal development.[14] More than 80% of the retinal cells were rhodopsin positive at P9, and the most of these cells were double positive for rhodopsin and CD73 (Fig. 1F), which suggests that CD73 is a marker of rhodopsin-positive cells. Previous reports demonstrated the expression of 5′-nucleotidase enzyme activities in photoreceptor cells of the rat retina,[15] which is consistent with our present results. Therefore, we examined in more detail the coexpression of CD73 and rhodopsin during retinal development. Retinal cells from mice at P1, P6, and P9 were dissociated and immunostained with the anti-CD73 and anti-rhodopsin antibodies. Some of the cells were replated and used for immunohistochemistry with the same set of antibodies (Fig. 1E). Less than 30% of the $CD73^+$ cells expressed rhodopsin in P1 mouse retinas, and more than 50% of the $CD73^+$ cells expressed rhodopsin in P6 mouse retinas. Interestingly, although a significant number of $CD73^+$ cells were observed at P6, not all cells were rhodopsin-positive cells at this stage (Fig. 1F). At the more advanced stage of P9, most of the cells were double-positive for CD73 and rhodopsin (Figs. 1E, 1F), and less than 10% of the cells in the P9 and adult samples were rhodopsin-positive/CD73-negative. We attempted to characterize these cells; however, we have no explanation for our observation. Taken together, these results suggest that retinal cells that commit to the rod photoreceptor cell lineage initially express CD73 and subsequently become double-positive for CD73 and rhodopsin. To examine this hypothesis at the transcriptional level, we examined the temporal transitions of mRNA expression of CD73 and rhodopsin by semiquantitative RT-PCR (see Fig. 4C). Weak expression of CD73 mRNA was observed in the retina at E16, and the strength was increased until P5, which is consistent with the transition of CD73 protein expression revealed by FACS analysis. This suggests that the expression of CD73 is regulated mainly at the transcriptional level. The onset of CD73 expression occurred earlier than that of rhodopsin, which supports the idea that CD73 is an earlier marker than rhodopsin of the photoreceptor lineage.

We also examined the spatial localization of $CD73^+$ cells in the developing retina by immunohistochemistry and compared this expression pattern with that of rhodopsin (Fig. 1G). In P1 retinas, CD73 was observed in the outer half of the neuroblastic layer, which corresponds to the area in which the photoreceptors start to differentiate. At P5, the ONL became visible, and CD73 expression was evident throughout the ONL. When we examined adult mouse-derived retinas, CD73 expression was strong and widespread in the ONL nucleus and in the outer region of the nucleus, and rhodopsin expression was strong in the outer region of the ONL, which corresponds to the outer segment of the photoreceptor. Although a previous study reported the expression of CD73 in Müller glial cells,[16] we did not observe the expression of CD73 in the inner nuclear layer (INL), in which the Müller glial cell body is

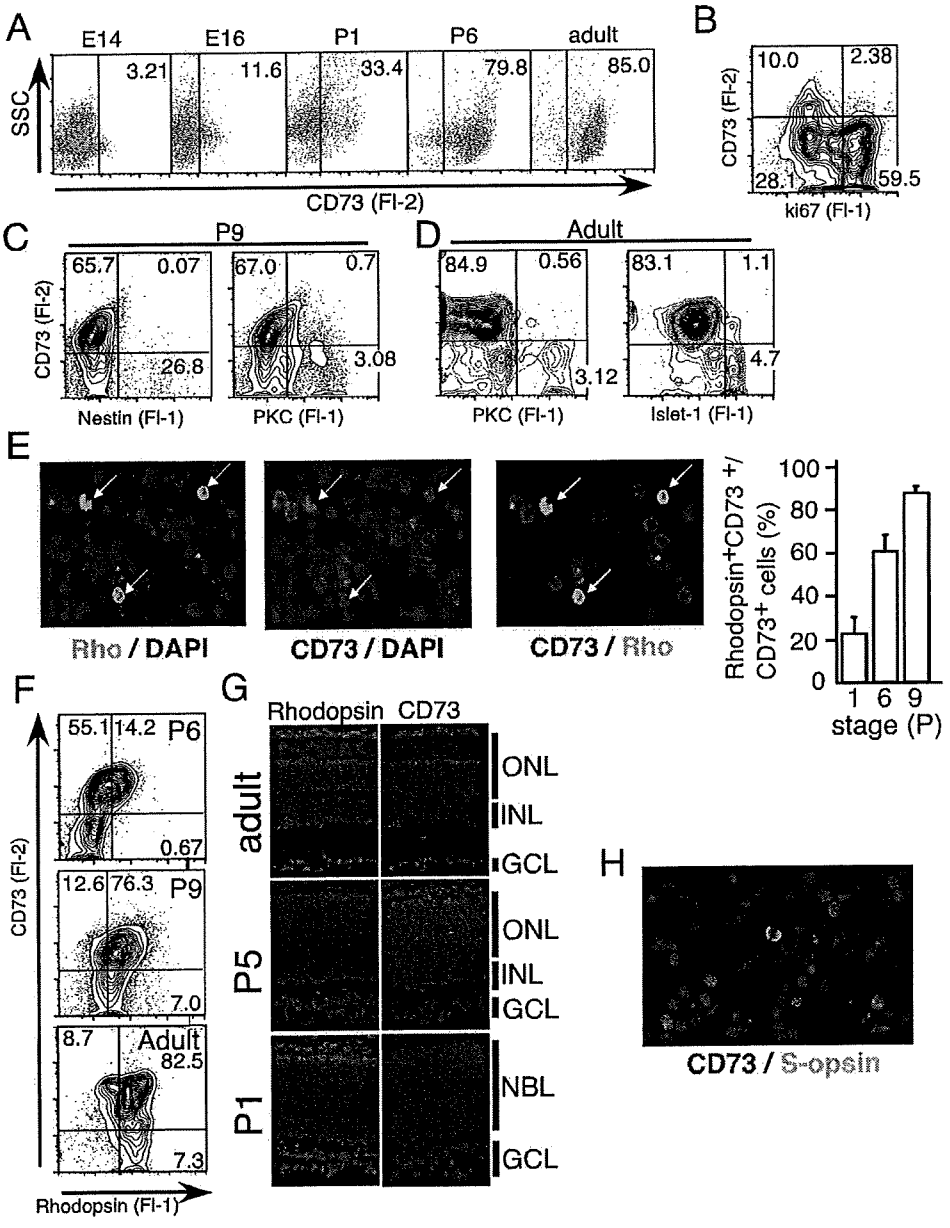

FIGURE 1. Characterization of CD73 expression. (A) Flow cytometric analysis of the expression of CD73 at various developmental stages of the mouse retina. The dot plot patterns of side scatter (SSC) versus CD73 are shown. (B–D) Contour plot patterns of double staining of the mouse retina at P1 with anti- CD73 versus anti-Ki67 (B), and of the mouse retina at the P9 stage with antibodies against nestin, protein kinase C (PKC) (C), and at the adult stage with antibodies against PKC and islet-1 (D). (E) Co-expression of CD73 (*red*) and rhodopsin (*green*) in dissociated retinal cells was examined. Retinal cells at the indicated stages were dissociated on the plate and immunostained with anti-CD73 and anti-rhodopsin antibodies. DAPI was used to stain the nuclei. *Left*: views under the microscope of samples derived from P9 mice. *Right*: the percentages of rhodopsin/CD73 double-positive subpopulation of $CD73^+$ cells are shown. (F) Contour plot pattern of double-staining for CD73 and rhodopsin of a retina at P6, P9, and adult. (G) Immunostaining for CD73 and rhodopsin of frozen-sectioned retina derived from mice at P1, P5, and adulthood. GCL, ganglion cell layer; NBL, neuroblastic layer; INL, inner nuclear layer; ONL, outer nuclear layer. (H) Double-staining of mouse retinal cells at the P2 stage with anti-CD73 (*red*) and anti-s-opsin (*green*) antibodies.

localized, at any of the stages examined (Fig. 1G and data not shown). This notion was confirmed by the lack of expression of mRNA of glutamine synthetase (GS), which is a marker of Müller glial cells, in the purified $CD73^+$ cell population (see Fig. 4A). Because GS antibody cannot be used for FACS analysis (data not shown), we examined its expression in dissociated $CD73^+$ retinal cells derived from P15 mice and found that only a negligible number (1/150 $CD73^+$ cells) of GS/CD73 double-positive cells was observed, further supporting this notion. In the ONL, in addition to the rod cells, cone cells were detected. We examined whether CD73 was expressed in cone cells by double immunostaining the adult mouse retina with the cone marker s-opsin and CD73. We found that $CD73^+$ cells never expressed s-opsin (Fig. 1H). However, when we used semiquantitative RT-PCR to examine the expression of s-opsin mRNA in $CD73^+$ and $CD73^-$ cells from the retinas of developing mice, s-opsin expression was observed in both cell fractions (see Fig. 4B).

In Vitro Differentiation and Proliferation of $CD73^+$ Cells

We next examined the differentiation and proliferation activities of isolated $CD73^+$ cells using an in vitro culture system. We used reaggregation cultures, which have been shown to be an excellent model system for examining the intrinsic proliferation and differentiation of retinal progenitors in vitro.[4,5] In this system, the cells proliferate and differentiate into rod photoreceptor cells in a manner similar to that seen in vivo.[17] By culturing labeled donor cells with an excess number of unlabeled host retinal cells, we could evaluate the intrinsic proliferation and differentiation of the donor cells in a defined environment.[18] To distinguish transplanted cells from host cells, we used neural retinas derived from EGFP transgenic (Tg) mice[8,9] as donor cells.[4,5] $CD73^+$ and $CD73^-$ cells of EGFP Tg mice at P1 were purified in a cell sorter (Fig. 2A) and mixed with an excess number of dissociated unfractionated host retinal cells from normal mice at P1 to prepare reaggregation

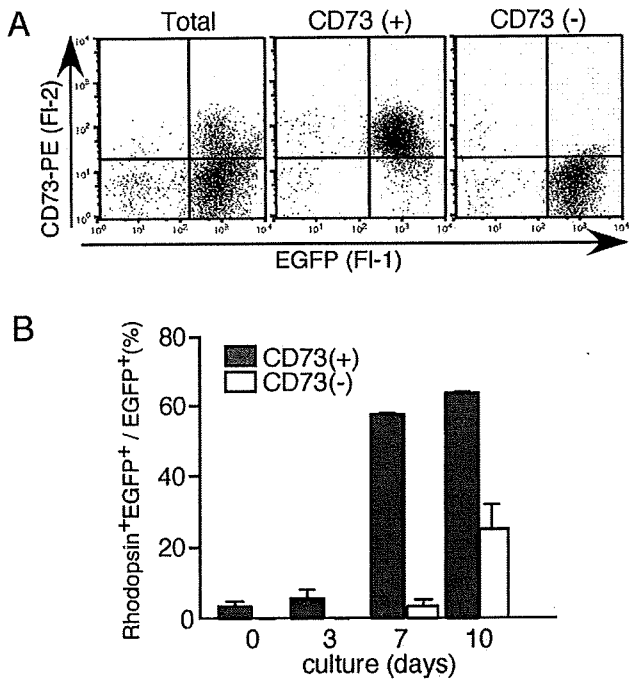

FIGURE 2. Differentiation of $CD73^+$ and $CD73^-$ cells in reaggregation cultures. (**A**) Dot plot pattern of EGFP (Fl-1) versus anti-CD73 antibody staining (PE [Fl-2]) of E17 neural retina derived from EGFP Tg mice. Whole cells displaying the pattern shown on the *left* were fractionated according to CD73 expression in the cell sorter, as shown in the *middle* ($CD73^+$) and *right* ($CD73^-$) panels. The purities of the fraction were approximately 90% and >95%, respectively. (**B**) Reaggregation cultures that consisted of a mixture of donor cells and host cells were prepared to analyze the differentiation of $CD73^+$ and $CD73^-$ cells. $CD73^+$ or $CD73^-$ retinal cells derived from the EGFP Tg mice at P1 were mixed with a large excess of retinal cells from normal mice of the same age. The rhodopsin-expressing cells (%) in the EGFP-positive cell population are shown. Reaggregation cultures were harvested at the indicated days of culture, and the cells were replated on a chamber glass slide and immunostained with antibodies against GFP and rhodopsin. The experiments were performed at least twice, with essentially the same results.

cultures. When we examined the expression of rhodopsin before starting the culture, less than 5% of $CD73^+$ cells were rhodopsin positive, but no expression of rhodopsin was observed in $CD73^-$ cells (Fig. 2B). After 3 days of culture, the number of rhodopsin-positive cells increased, but these cells were still only observed in the $CD73^+$ cell reaggregates. On day 7 of culture, nearly 60% of the $CD73^+$ cells were rhodopsin positive, whereas only a low percentage of the $CD73^-$ cells were rhodopsin positive. In this culture system, the efficiency of cell differentiation was lower than in the in vivo situation (using unfractionated retinal cells, the maximum percentage we observed as rhodopsin-positive cells was 60%; data not shown). On day 10 of culture, although the proportion of rhodopsin-positive cells in the $CD73^-$ cell population had increased significantly, it was far lower than the proportion of rhodopsin-positive cells in the $CD73^+$ population. This indicates that $CD73^+$ cells are in a more advanced stage of the rod photoreceptor cell lineage than $CD73^-$ cells.

Role of CD73 in Retinal Rod Photoreceptor Cell Differentiation

CD73 is an enzyme with ecto-5′-nucleotidase activity, and the enzymatic product of CD73 is adenosine.[6,7] Of the four types of adenosine receptor (A1, A2a, A2b, A3),[19] A2a and A2b have previously been reported to be expressed in the neural retina of the rat.[20,21] We examined the temporal expression of the mRNAs for these receptors by semiquantitative RT-PCR (Fig. 3A). We found that A1 was expressed in the neural retina from an early stage (E16) of retinal development and that the A1 expression level increased as retinal development progressed (Fig. 3A). Very weak bands were observed for A2a and A2b in the embryonic retina; these receptors started to be expressed in the postnatal retina, and the expression level increased concomitantly with development. We also used semiquantitative RT-PCR of RNA samples isolated from purified $CD73^+$ and

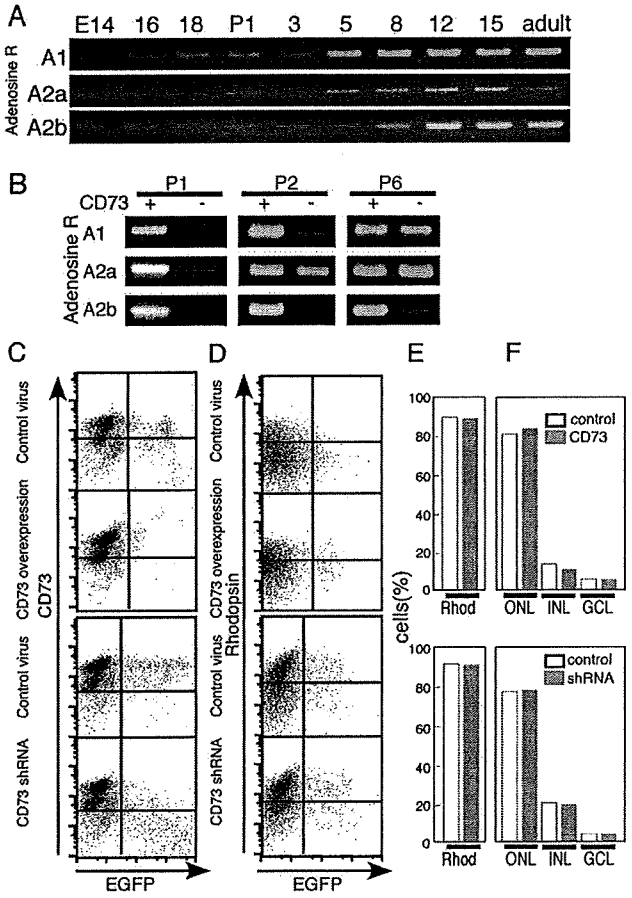

FIGURE 3. The roles of CD73 in retinal development. Temporal expression of mRNA for adenosine receptors in the developing retina. (**A**) Semiquantitative RT-PCR for adenosine receptors A1, A2a, and A2b was carried out using total RNA samples purified from mouse retinas at various developmental stages. (**B**) The expression of adenosine receptors A1, A2a, and A2b in $CD73^+$ and $CD73^-$ cells at the indicated stages was examined by semiquantitative RT-PCR. (**C–F**) Gain- and loss-of-function analyses of CD73. Retroviruses that encode IRES-EGFP or CD73-IRES-EGFP (for overexpression experiments) and CMV EGFP or shRNA against CD73-CMV EGFP (for downregulation experiments) were transduced into retinal explants at E16, followed by FACS analysis of the expression of CD73 (**C**) and rhodopsin (**D**) after 14 days of culture. (**E**) Quantitative results for rhodopsin-positive cells calculated from (**D**). The rhodopsin-positive cells in the EGFP-positive cell population (shown in **D**) are expressed as the relative percentage of those in the EGFP-negative cells population in each experiment. (**F**) Distributions of EGFP-positive cells in the ONL, INL, and GCL. Retroviruses that encode IRES-EGFP, CD73-IRES-EGFP, CMV-EGFP, or shRNA against CD73-CMV EGFP were transduced into retinal explants at E16. After 14 days of culture, frozen sections were produced, and the distribution of EGFP-positive cells in each layer was examined.

$CD73^-$ cells at various stages to examine whether these receptors were expressed in $CD73^+$ cells (Fig. 3B). Interestingly, all three adenosine receptor subtypes were predominantly expressed in $CD73^+$ cells at P1 (Fig. 3B). At P2, weak expression of all three receptors was observed in the $CD73^-$ cells; at P6, significant expression of A1 and A2a was observed in both the $CD73^+$ and $CD73^-$ cells, and A2b was detected primarily in the $CD73^+$ fraction.

To examine the role of CD73 in retinal development, we performed gain- and loss-of-function analyses of CD73 using retinal explant culture. For the gain-of-function analysis, CD73 was expressed by retrovirus-mediated gene expression in the retinal explant. A retrovirus that encoded the wild-type CD73-IRES-EGFP was transduced into retinal explants prepared from an E16 mouse. After 14 days of culture, CD73 expression was examined by FACS analysis (Fig. 3C). The control EGFP virus-expressing population contained both $CD73^+$ and $CD73^-$ cells. In contrast, the CD73-IRES-EGFP virus-transduced cell population contained only $CD73^+$ cells (Fig. 3C). In addition, the expression level of CD73 in this cell population was higher than that of the control samples. After 14 days of retinal explant culture, the expression of rhodopsin was examined by FACS analysis (Figs. 3D, 3E). In the CD73-overexpressed fraction, the proportion of rhodopsin-positive cells was similar to that observed in the control EGFP virus-infected population (Fig. 3E). The downregulation of CD73 was achieved using shRNA, which was introduced into the retinal explant cultures by retroviruses. The suppression of CD73 expression was confirmed by FACS analysis (Fig. 3C). The levels of rhodopsin expression were similar in the EGFP-positive and EGFP-negative cells after 14 days of culture (Fig. 3D). Once again, the levels of rhodopsin expression (Fig. 3E) and distribution of cells into subretinal layers (Fig. 3F) were similar in the EGFP-positive, CD73-downregulated cells and the control EGFP virus-infected cells. Taken together, these results suggest that CD73 does not mediate autonomous cellular signals to promote rhodopsin lineage differentiation. We also examined whether the overexpression or downregulation of CD73 affects other cell lineages, such as Müller glia, ganglion, and amacrine cells by immunostaining with specific markers such as glutamine synthetase and HuC/D. We did not detect significant differences between the two fractions and the controls (data not shown).

CD73 Expressed Downstream of Crx

To analyze the detailed molecular mechanisms, we examined the gene expression patterns of $CD73^+$ and $CD73^-$ cells by semiquantitative RT-PCR. As expected, rhodopsin was expressed exclusively in $CD73^+$ fractions (Fig. 4B). Crx and Nrl are transcription factors that play important roles in photoreceptor cell development.[22,23] Nrl was observed exclusively in $CD73^+$ cells, whereas Crx was observed in both $CD73^+$ and negative cells, which suggests that Crx is expressed earlier than CD73. We also examined the expression of early retinal progenitor markers, such as Chx10[24] and Hes1, and found that they were expressed exclusively in $CD73^-$ cells, as expected (Fig. 4A).

We examined in more detail the time course of gene expression (Fig. 4C). We first examined the temporal transitions of mRNA expression of CD73 and rhodopsin by semiquantitative RT-PCR (Fig. 4C). Weak expression of CD73 mRNA was observed in the retina at E16, and the strength was increased until P5, which is consistent with the transition of CD73 protein expression revealed by FACS analysis. This suggests that the expression of CD73 is regulated mainly at the transcriptional level. The onset of CD73 expression occurred earlier than that of rhodopsin, which supports the idea that CD73

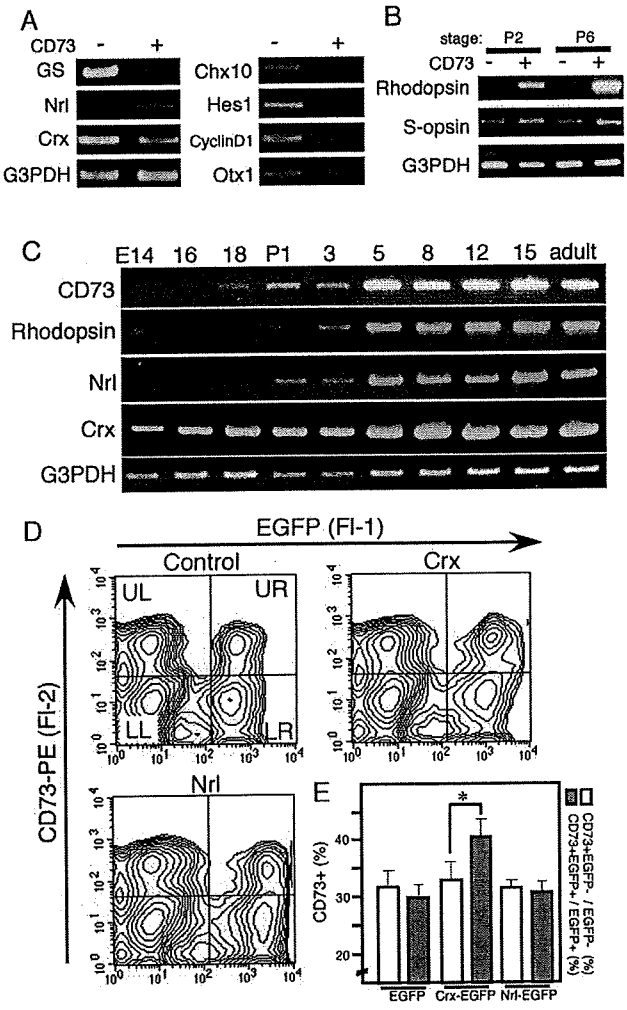

FIGURE 4. Mapping of CD73 in the hierarchy of genes involved in photoreceptor cell differentiation. (**A**, **B**) Semiquantitative RT-PCR of $CD73^+$ and $CD73^-$ populations from the P1 (**A**) and P2 and P6 (**B**) mouse retina. The RT-PCR products were separated in a 1% agarose gel and visualized with ethidium bromide. G3PDH was used as a control. The experiments were performed at least twice, for all the primers, using independently prepared samples, with essentially the same results. (**C**) Kinetics of gene expression in the mouse retina. Semiquantitative RT-PCR was performed using RNA from mouse retinas at various developmental stages. G3PDH was used as a control. (**D**, **E**) Effects of retrovirus-mediated expression of Crx and Nrl transcription factors on CD73 expression. Retinal explant cultures prepared from E16 mouse retinas were infected with retroviruses that contained EGFP, Crx-IRES-EGFP, or Nrl-IRES-EGFP, and the cells were cultured for 4 days and then dissociated. The expression of CD73 in the EGFP-positive and EGFP-negative cells was examined by flow cytometry. The flow cytometric patterns (**D**) and the calculated values for the $CD73^+$ cells in the EGFP-positive or EGFP-negative populations are shown (**E**). The experiments were performed at least three times with essentially the same results.

is an earlier marker than rhodopsin of the photoreceptor lineage. Crx was found to be expressed even at E14, and CD73 expression started around E16 to E18. A transition in Nrl expression in the developing mouse retina was previously reported. Bibb et al.[25] reported that Nrl was expressed after birth, whereas Akimoto et al.[26] reported that Nrl was first expressed during early embryogenesis around E12. In our study, Nrl and rhodopsin expression began around P1. The difference in Nrl expression between these previous studies

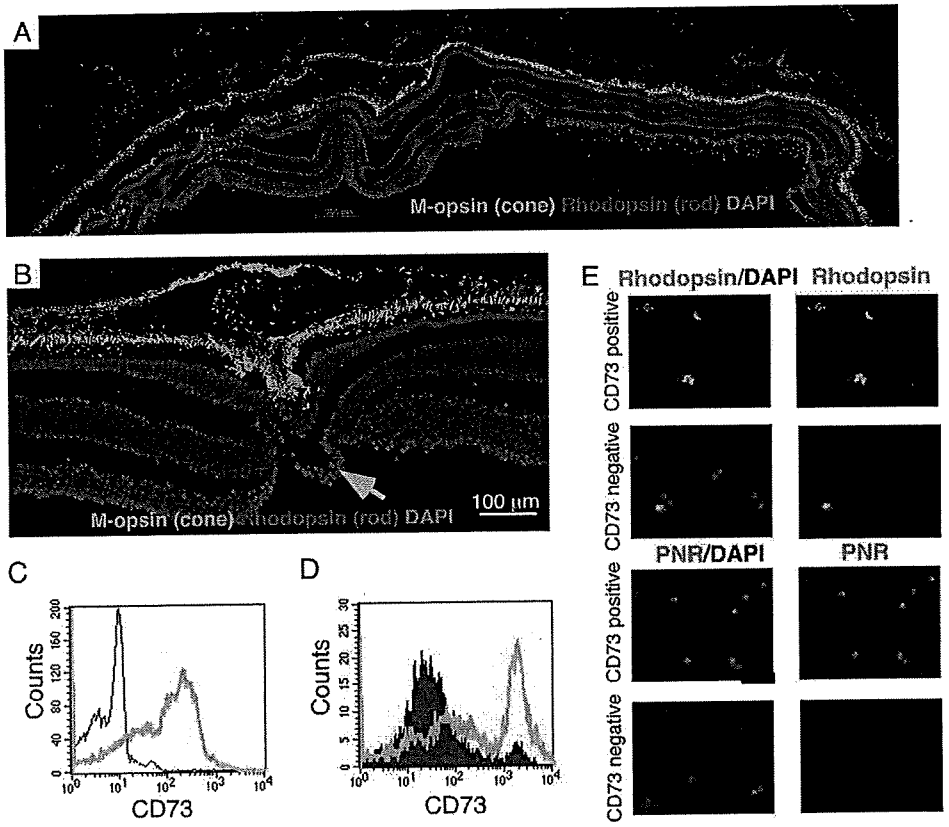

FIGURE 5. Expression of CD73 in marmoset retina. (A, B) Expression of M-opsin and rhodopsin in adult common marmoset retina. Immunostaining was performed using frozen-sectioned retina, and nuclei were visualized by DAPI. (C) FACS pattern of CD73 staining of whole retina of adult common marmoset. *Green line*: CD73 staining. *Black line*: control IgG staining. (D) Adult common marmoset retina was mechanically divided into fovea and other regions, and FACS analysis of CD73 expression was performed for both fractions. *Violet region, green line*: staining patterns of fovea and other regions, respectively. (E) Whole retina of adult common marmoset was dissociated and sorted to $CD73^+$ and $CD73^-$ populations by cell sorter, and the cells were replated on a chamber glass slide and immunostained with antibodies against rhodopsin (*upper four panels*) and PNR (*lower four panels*). Nuclei were stained with DAPI.

and our own may be attributed to a difference in primer sensitivity. Our results confirm that the onset of CD73 expression occurs between Crx and Nrl expression. Therefore, we examined the role of Crx in CD73 expression. To test the effects of Crx, we used Nrl for comparison purposes and incorrectly expressed these genes in retinal explants derived from E16 mice by retroviral-mediated gene transfer.[11] Retinal explants were infected with retrovirus that encoded Crx- or Nrl-IRES-EGFP; they were cultured for 4 days, harvested, and dissociated. CD73 expression was analyzed by flow cytometry (Figs. 4D, 4E). In the control EGFP virus-transfected cells, approximately 30% of the cells expressed CD73 in both the EGFP-positive and EGFP-negative fractions. However, in the Crx retrovirus-infected explant samples, more than 40% of the EGFP-expressing cells also expressed CD73, which was significantly higher than that of the control cells (Fig. 4E). In the Nrl-expressing cell population, the proportion of $CD73^+$ cells in the EGFP-positive fraction was almost the same as in the uninfected parental cells or control EGFP virus-infected cells (Figs. 4D, 4E). Taken together, these results suggest that the activation of Crx positively regulates CD73-expressing cells and that Crx (but not Nrl) is upstream of CD73 in the photoreceptor development hierarchy.

CD73, a Marker for Rod Photoreceptor Cells in Retina of Common Marmoset (*Callithrix jacchus*)

Finally, we asked whether our finding that CD73 is a marker for rod photoreceptor is also applicable for primates. Retinas from adult common marmoset were isolated, and we first examined the expression of rhodopsin and M-opsin in the frozen sectioned retina, including the fovea region. The fovea pit is depicted at the central region of Figure 5A, identified by its unique bended structure of nuclear layers (Fig. 5B). As previously reported,[27] M-opsin was predominantly expressed in the fovea region, and, in contrast, rhodopsin was distributed in regions other than the fovea (Figs. 5A, 5B). Although anti-human CD73 antibody did not give reliable signals of frozen sectioned retina by immunohistochemistry, FACS analysis using whole retina showed strong expression of CD73 (Fig. 5C). Therefore, under a microscope, we mechanically divided the fovea and other regions with the use of a scalpel and used FACS to examine the CD73 expression of these two fractions (Fig. 5D). Strong CD73 expression was observed with retina except for fovea, and only a small population of cells at the foveal region expressed CD73. We purified $CD73^+$ and $CD73^-$ cells of the adult marmoset retina by cell sorter, and the cells were seeded on the slide glass and immunostained of the purified cells with anti-rhodopsin and -PNR, which is rod photoreceptor specific marker, antibodies (Fig. 5E). Almost all cells in $CD73^+$ fractions were rhodopsin or PNR positive; in contrast, only a few positive cells were observed in $CD73^-$ cells. Taken together, we concluded that CD73 is a marker of rod photoreceptor cells in the mature retina of the common marmoset.

DISCUSSION

In the present study, we show that CD73 labels precursor and mature populations of photoreceptor cells. The present report is the first to show specific expression of a cell surface molecule in a photoreceptor cell lineage and the application of this molecule for the enrichment of photoreceptor precursor cells. This is important in terms of applications related to transplantation for the treatment of retinal diseases. Using reaggregation cultures of retinal cells, we show that the purification of CD73 is an efficient way to achieve photoreceptor cell generation by transplantation. This is an in vitro model system, and we are in the process of developing an in vivo transplantation system.

Recently, in vivo retinal repair by transplantation of photoreceptor precursors has been reported.[3] Successful regeneration of functional rod photoreceptors in the mouse is encouraging for researchers working on regenerative medicine of the neural retina. However, in the previous report, the isolated retinas were from transgenic mice that expressed EGFP under the control of the Nrl promoter, which limits the use of this protocol for human applications. CD73 is a cell surface molecule and an anti-CD73 antibody is commercially available, allowing for transplantation and regeneration using CD73-expressing cells without risk for gene transfer. Furthermore, it is important that we found that CD73 is also a marker for the common marmoset photoreceptor. Thus, we can apply this knowledge easily and immediately to human systems using an anti-human CD73 antigen antibody.

Our observation of exclusive expression of CD73 in a photoreceptor lineage is supported by recent DNA microarray analyses of knockout mice. In Nrl-knockout and rhodopsin-knockout mice, both of which lack rod photoreceptors, DNA microarray analyses comparing the retinas of wild-type mice and the knockout mice have revealed that the expression of CD73 is downregulated in these knockout mice.[28,29] However, previous reports have suggested that the 5′-nucleotidase activity is localized in photoreceptor cells and in Müller cells.[30,31] More recently, immunostaining of the 5′-nucleotidase with polyclonal antibody in the developing retina of the mouse has concluded that this enzyme is distributed in Müller cells.[16] In contrast, we did not observe the expression of CD73 in the INL, where the nuclei of Müller glial cells are localized, and CD73 expression never overlapped with glutamine synthetase expression, which is a marker of Müller glial cells, thereby suggesting that CD73 is not expressed in Müller glial cells. Because the previous report did not describe double immunostaining for the 5′-nucleotidase and markers of retinal cells,[16] it is not possible to compare directly the previous results with our present results. However, given that the polyclonal antibody used in the previous paper was raised against the soluble form of bovine 5′-nucleotidase,[16] it is possible that the antibody recognizes a molecule different from that recognized by the anti-CD73 monoclonal antibody used in our present study. This notion is supported by their observation that the expression of the antigen during embryonic development was also associated with proliferating cellular elements,[16] which contrasts with our finding that CD73 is expressed exclusively in nonproliferating cells. Nevertheless, we cannot exclude the possibility that the tertiary structure of CD73 is different in different cell types and that the antibodies only recognize a certain structure of CD73.

Initially, we expected that cone-specific genes would not be expressed in $CD73^+$ cells. However, cone s-opsin mRNA was detected in CD73 cells derived from neonatal mice. In contrast, in mature retinas, we did not observe CD73 expression in s-opsin-expressing cone cells. We speculate that the transition of CD73 expression during photoreceptor cell differentiation occurs as shown schematically in Figure 6. Thus, CD73 is expressed in the common progenitors of cone and rod cells. After terminal differentiation, CD73 continues to be expressed in rod cells until adulthood, whereas it is downregulated in the cone cell lineage.

Nrl and Crx are key transcriptional factors that control photoreceptor differentiation.[23] The homeodomain protein Crx is required for both rod and cone differentiation and regulates the transcription of many photoreceptor-specific genes.[32] The Maf-family bZIP transcription factor NRL is essential for rod differentiation and controls the expression of most of the rod-specific genes.[23] Based on our observations of differential expression of Crx and Nrl in $CD73^+$ and $CD73^-$ cells, we hypothesize that CD73 is downstream of Crx and upstream or parallel to Nrl in rod cell differentiation. Furthermore, detailed examination of the transition of expression of the mRNAs for Crx, CD73, and Nrl also support the idea of ordered expression of these genes in the developing retina. Previous studies of the promoter for CD73 in humans have revealed the involvement of various immune-related transcription factors such as NFAT, hypoxia-related factor 1, and the Wnt signaling pathway.[33,34] We looked for the Crx consensus-binding sequence (C/T TAATCC[35]) in approximately 1 kb of the 5′ upstream region of the mouse CD73 gene and found one matching sequence at −870 nt from the initiation codon. However, this sequence was not found within the region covering 1 kb of human CD73 5′ upstream. We do not know whether the enhancement of CD73-expressing cells by Crx is due to the direct effects of Crx on CD73 transcription or simply results from an expanded population of rod photoreceptors. The most important outcome of the present study is that CD73 is a marker for cells at defined stages of the photoreceptor lineage and can be used in the isolation and transplantation of these cell populations.

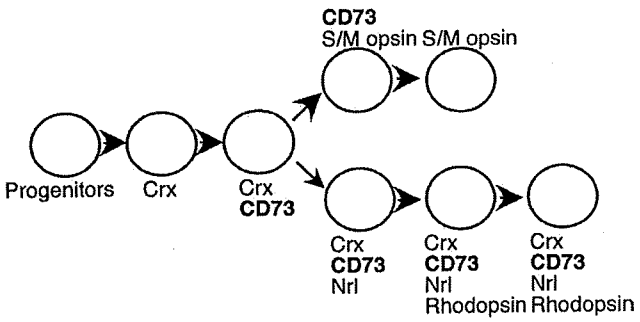

FIGURE 6. Schematic representation of photoreceptor cell differentiation and CD73. CD 73 is first expressed after Crx in the common precursors of the rod and cone cells and continues to be expressed in the rod cell lineage. However, CD73 appears to be downregulated once the cells commit to differentiation into the cone cell lineage.

Acknowledgments

The authors thank Yasuo Ouchi for helpful discussions, and Takashi Shibata and Nobukazu Watanabe of the FACS Core Laboratory (Institute of Medical Science, University of Tokyo, Tokyo, Japan) for technical support with the sorting.

References

1. Rattner A, Nathans J. Macular degeneration: recent advances and therapeutic opportunities. *Nat Rev Neurosci.* 2006;7:860–872.
2. Hartong DT, Berson E, Dryja TP. Retinitis pigmentosa. *Lancet.* 2006;368:1795–1809.
3. MacLaren RE, Pearson RA, MacNeil A, et al. Retinal repair by transplantation of photoreceptor precursors. *Nature.* 2006;444.
4. Koso H, Ouchi Y, Tabata Y, et al. SSEA-1 marks regionally restricted immature subpopulations of embryonic retinal progenitor cells. *Dev Biol.* 2006;292:265–276.
5. Koso H, Satoh S, Watanabe S. c-Kit marks late retinal progenitor cells and regulates their differentiation in developing mouse retina. *Dev Biol.* 2007;301.
6. Zimmermann H. 5′-Nucleotidase: molecular structure and functional aspects. *Biochem J.* 1992;285:345–365.
7. Deussen A, Bading B, Kelm M, Schrader J. Formation and salvage of adenosine by macrovascular endothelial cells. *Am J Physiol.* 1993; 264:692–700.
8. Okabe M, Ikawa M, Kominami K, Nakanishi T, Nishimune Y. 'Green mice' as a source of ubiquitous green cells. *FEBS Lett.* 1997;407:313–319.

9. Ikawa M, Yamada S, Nakanishi T, Okabe M. Green fluorescent protein (GFP) as a vital marker in mammals. *Curr Top Dev Biol.* 1999;44:1-20.
10. Tabata Y, Ouchi Y, Kamiya H, Manabe T, Arai K, Watanabe S. Retinal fate specification of mouse embryonic stem cells by ectopic expression of Rx/rax, a homeobox gene. *Mol Cell Biol.* 2004;24:4513-4521.
11. Ouchi Y, Tabata Y, Arai K, Watanabe S. Negative regulation of retinal-neurite extension by β-catenin signalling pathway. *J Cell Sci.* 2005;118:4473-4483.
12. Gerdes J, Schwab U, Lemke H, Stein H. Production of a mouse monoclonal antibody reactive with a human nuclear antigen associated with cell proliferation. *Int J Cancer.* 1983;31:13-20.
13. Lendahl U, Zimmerman LB, McKay RD. CNS stem cells express a new class of intermediate filament protein. *Cell.* 1990;60:585-595.
14. Marquardt T, Gruss P. Generating neuronal diversity in the retina: one for nearly all. *Trends Neurosci.* 2002;25:32-38.
15. Takizawa T. 5'-Nucleotidase in rat photoreceptor cells and pigment epithelial cells processed by rapid-freezing enzyme. *J Histochem Cytochem.* 1998;46:1091-1095.
16. Braun N, Brendel P, Zimmerman H. Distribution of 5'-nucleotidase in the developing mouse retina. *Dev Brain Res.* 1995;88:79-86.
17. Watanabe T, Raff MC. Rod photoreceptor development in vitro: intrinsic properties of proliferating neuroepithelial cells change as development proceeds in the rat retina. *Neuron.* 1990;4:461-467.
18. Belliveau MJ, Cepko CL. Extrinsic and intrinsic factors control the genesis of amacrine and cone cells in the rat retina. *Development.* 1999;126:555-566.
19. Yaar R, Jones MR, Chen J-F, Ravid K. Animal models for the study of adenosine receptor function. *J Cell Physiol.* 2005;202:9-20.
20. Yang D, Zhang Y, Nguyen HG, et al. The A2B adenosine receptor protects against inflammation and excessive vascular adhesion. *J Clin Invest.* 2006;116:1913-1923.
21. Kvanta A, Seregard S, Sejersen S, Kull B, Fredholm BB. Localization of adenosine receptor messenger RNAs in the rat eye. *Exp Eye Res.* 1997;65:595-602.
22. Furukawa T, Morrow EM, Li T, Davis FC, Cepko CL. Retinopathy and attenuated circadian entrainment in Crx-deficient mice. *Nat Genet.* 1999;23:466-470.
23. Mears AJ, Kondo M, Swain PK, et al. Nrl is required for rod photoreceptor development. *Nat Genet.* 2001;29:447-452.
24. Burmeister M, Novak J, Liang M-Y, et al. Ocular retardation mouse caused by Chx10 homeobox null allele: impaired retinal progenitor proliferation and bipolar cell differentiation. *Nature.* 1996;12:376-384.
25. Bibb LC, Holt JK, Tarttelin EE, et al. Temporal and spatial expression patterns of the Crx transcription factor and its downstream target: critical differences during human and muse eye development. *Hum Mol Genet.* 2001;15:1571-1579.
26. Akimoto M, Cheng H, Zhu D, et al. Targeting of GFP to newborn rods by Nrl promoter and temporal expression profiling of flow-sorted photoreceptors. *Proc Natl Acad Sci U S A.* 2006;103:3890-3895.
27. Martin PR, Grunert U. Analysis of the short wavelength-sensitive ("Blue") cone mosaic in the primate retina: comparison of new world and old world monkeys. *J Comp Neurol.* 1999;406:1-14.
28. Yoshida S, Mears AJ, Fiedman JS, et al. Expression profiling of the developing and mature Nrl−/− mouse retina: identification of retinal disease candidates and transcriptional regulatory targets of Nrl. *Hum Mol Genet.* 2004;13:1487-1503.
29. Kennan A, Aherne A, Palfi A, et al. Identification of an IMPDH1 mutation in autosomal dominant retinitis pigmentosa (RP10) revealed following comparative microarray analysis of transcripts derived from retinas of wild-type and Rho (−/−) mice. *Hum Mol Genet.* 2002;11:547-557.
30. Kreutzberg GW, Hussain ST. Cytochemical heterogeneity of the glial plasma membrane: 5'-nucleotidase in retinal Muller cells. *J Neurocytol.* 1982;11:53-64.
31. Kreutzberg GW, Hussain ST. Cytochemical localization of 5'-nucleotidase activity in retinal photoreceptor cells. *Neuroscience.* 1984;11:857-866.
32. Furukawa T, Morrow EM, Cepko CL. Crx, a novel otx-like homeobox gene, shows photoreceptor-specific expression and regulates photoreceptor differentiation. *Cell.* 1997;91:531-541.
33. Spychala J, Kitajewski J. Wnt and beta-catenin signaling target the expression of ecto-5'-nucleotidase and increase extracellular adenosine generation. *Exp Cell Res.* 2004;296:99-108.
34. Synnestvedt K, Furuta GT, Comerford KM, et al. Ecto-5'-nucleotidase (CD73) regulation by hypoxia-inducible factor-a mediates permeability changes in intestinal epithelia. *J Clin Invest.* 2002;110:993-1002.
35. Chen S, Wang QL, Nie Z, et al. Crx, a novel Otx-like paired-homeodomain protein, binds to and transactivates photoreceptor cell-specific genes. *Neuron.* 1997;19:1017-1030.

Nongenetic method for purifying stem cell–derived cardiomyocytes

Fumiyuki Hattori[1,2], Hao Chen[1,3], Hiromi Yamashita[1], Shugo Tohyama[1,3], Yu-suke Satoh[1,4], Shinsuke Yuasa[1], Weizhen Li[1], Hiroyuki Yamakawa[1,3], Tomofumi Tanaka[1,2], Takeshi Onitsuka[1,3], Kenichiro Shimoji[1,3], Yohei Ohno[1,3], Toru Egashira[1,3], Ruri Kaneda[1], Mitsushige Murata[1,3], Kyoko Hidaka[5], Takayuki Morisaki[5], Erika Sasaki[6], Takeshi Suzuki[4], Motoaki Sano[1], Shinji Makino[1], Shinzo Oikawa[2] & Keiichi Fukuda[1]

Several applications of pluripotent stem cell (PSC)-derived cardiomyocytes require elimination of undifferentiated cells. A major limitation for cardiomyocyte purification is the lack of easy and specific cell marking techniques. We found that a fluorescent dye that labels mitochondria, tetramethylrhodamine methyl ester perchlorate, could be used to selectively mark embryonic and neonatal rat cardiomyocytes, as well as mouse, marmoset and human PSC-derived cardiomyocytes, and that the cells could subsequently be enriched (>99% purity) by fluorescence-activated cell sorting. Purified cardiomyocytes transplanted into testes did not induce teratoma formation. Moreover, aggregate formation of PSC-derived cardiomyocytes through homophilic cell-cell adhesion improved their survival in the immunodeficient mouse heart. Our approaches will aid in the future success of using PSC-derived cardiomyocytes for basic and clinical applications.

Human embryonic stem cells (ESCs) and induced pluripotent stem cells (iPSCs) could prove to be an unlimited source of cardiomyocytes. Several studies have achieved directed differentiation of mouse, monkey and human ESCs into cardiomyocytes[1–3] but with variable efficiency. Some protocols describe up to 60% differentiation efficiency, but none achieve >99% of cells differentiating into cardiomyocytes without the use of genetic selection methods[4]. Transplantation of undifferentiated ESCs results in the formation of teratomas[5]. Thus, it is necessary to purify ESC-derived cardiomyocytes before transplantation.

ESC lines with various combinations of cardiomyocyte-specific reporters can be used to obtain highly pure ESC-derived cardiomyocytes[4,6–10], but this requires genetic modification of the cells. Also, discontinuous Percoll density gradient centrifugation could be used to enrich for mouse and human ESC-derived cardiomyocytes, but the purity of the cardiomyocytes in these preparations is relatively low[11,12]. Here we show that cardiomyocytes in early mouse embryos or those differentiated from pluripotent stem cells (PSCs) have high mitochondrial content and can be purified without the need for genetic modification, using fluorescent dyes that label mitochondria.

RESULTS

Characterization of mitochondrial dyes

In primary cultures of neonatal rat heart cells stained with MitoTracker Red (Invitrogen) the fluorescence intensity of cardiomyocytes was much higher compared to that of nonmyocytes (**Fig. 1a**). MitoTracker Red and tetramethylrhodamine methyl ester perchlorate (TMRM) specifically accumulated in both the subsarcomeric mitochondria, located around the nucleus and in the intermyofibrillar mitochondria (**Fig. 1a** and **Supplementary Fig. 1**). To confirm specific mitochondrial staining of MitoTracker dyes, we stained neonatal rat cardiomyocytes with MitoTracker Red and JC-1 (a mitochondrial voltage-sensitive dye; **Supplementary Fig. 2**).

Fluorescence-activated cell sorter (FACS) analysis of cells dissociated from neonatal heart revealed three main populations (**Fig. 1b**). We sorted the populations with the highest (designated as fraction 1), the middle (fraction 2) and the lowest (fraction 3) fluorescence intensity and cultured them separately. All the cells in fraction 1 showed rhythmic beating and were immunostained with an antibody to α-actinin (**Fig. 1c**), indicating they were cardiomyocytes. We identified very few cardiomyocytes in fraction 2 (**Fig. 1c**). Fraction 3 consisted of red blood cells and dead cells. We confirmed the neonatal rat cardiomyocyte content in fraction 1 by immunofluorescence staining for α-actinin to be 99.4 ± 0.6% (**Fig. 1d**), and the yield was approximately 5×10^5 cells from a single heart.

Next, we compared the efficacy of various mitochondrial dyes for separating the neonatal rat cardiomyocyte population from the nonmyocytes and found that TMRM was the most effective (**Fig. 1e,f**). We then evaluated the washout efficiencies of the dyes and found that TMRM disappeared completely within 24 h, whereas

[1]Department of Regenerative Medicine and Advanced Cardiac Therapeutics, Keio University School of Medicine, Tokyo, Japan. [2]Asubio Pharma Co., Ltd., Osaka, Japan. [3]Division of Cardiology, Department of Medicine, Keio University School of Medicine, Tokyo, Japan. [4]Division of Basic Biological Sciences, Faculty of Pharmacy, Keio University, Tokyo, Japan. [5]Department of Bioscience, National Cardiovascular Center Research Institute, Osaka, Japan. [6]Laboratory of Applied Developmental Biology, Marmoset Research Department, Central Institute for Experimental Animals, Kanagawa, Japan. Correspondence should be addressed to K.F. (kfukuda@sc.itc.keio.ac.jp).

RECEIVED 10 AUGUST; ACCEPTED 15 OCTOBER; PUBLISHED ONLINE 29 NOVEMBER 2009; DOI:10.1038/NMETH.1403

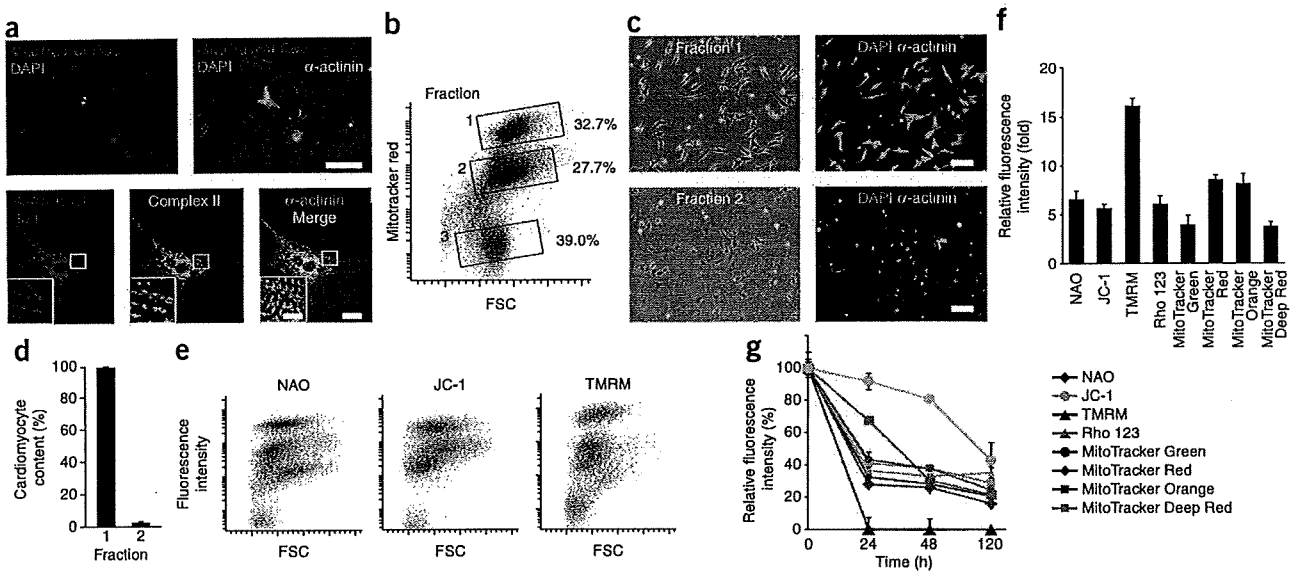

Figure 1 | Mitochondrial dyes for cardiomyocyte purification. (**a**) Fluorescence images of neonatal rat cardiomyocytes prestained with MitoTracker Red and immunostained for α-actinin (top) or prestained with MitoTracker Red and immunostained for mitochondrial electron transfer chain complex II (complex II) and α-actinin (bottom). DAPI, nuclear stain. Scale bars, 100 μm (top); 20 μm (bottom); and 10 μm (bottom inset). (**b**) FACS analysis of neonatal rat heart-derived cells stained with MitoTracker Red. The sorted cells were divided into fractions 1–3 (boxed). FSC, forward scatter. (**c**) Immunofluorescence staining for α-actinin of cells from fractions 1 and 2. Blue, DAPI staining. Scale bars, 100 μm. (**d**) Cardiomyocyte content in fractions 1 and 2. Data are shown as mean ± s.d. (n = 3). (**e**) Representative FACS plots of dissociated cells from neonatal rat heart stained with mitochondrial dyes. (**f**) Relative fluorescence intensity of the indicated mitochondrial dyes in fractions 1 versus 2. Data are shown as mean ± s.d. (n = 3). (**g**) Washout of the indicated mitochondrial dyes from neonatal rat cardiomyocytes. Data are shown as mean ± s.d. (n = 3).

other dyes remained for at least 5 d (**Fig. 1g** and **Supplementary Fig. 3a**). TMRM and JC-1 at 100 nM did not affect cell viability using 3-(4,5-dimethyl-thiazol-2-yl)-2,5-diphenyltetrazolium bromide (MTT) assay, whereas other dyes affected viability differently (**Supplementary Fig. 3b**). Based on these results, we selected TMRM for subsequent experiments.

Purification of cardiomyocytes from heart and whole embryos

To investigate the mitochondrial content of cardiomyocytes at different developmental stages, we performed FACS analysis of rat hearts at embryonic day 11.5 (E11.5) to postnatal day 8 (P8); the hearts had been dissociated and labeled with TMRM (**Fig. 2a**). The mean ratio of TMRM fluorescence in fraction 1 to fraction 2 gradually increased with increasing embryonic stage and rapidly after birth (**Fig. 2b**). FACS analysis followed by immunofluorescence staining confirmed over 99% cardiomyocyte purity at all stages (**Fig. 2c,d**).

We then stained live embryos (E11.5 and E12.5) with TMRM. The heart showed markedly stronger fluorescence compared with other tissues (**Fig. 2e** and **Supplementary Video 1**). Intraplacental injection of MitoTracker Red also resulted in the strongest accumulation of fluorescence in the heart via embryonic circulation. However, other tissues had much weaker fluorescence (**Supplementary Fig. 4**).

To assess why there was strong TMRM fluorescence in the embryonic heart, we compared expression levels of complex I–V of the 36 kDa mitochondrial outer membrane protein porin (also known as the voltage-dependent anion channel) and of heat shock protein 70 between cardiac and various noncardiac tissues in rat E12.5 embryos; we detected markedly stronger expression in the myocardium (**Supplementary Fig. 5**). Furthermore, immunostaining of the fetal heart area for α-actinin, manganese superoxide dismutase (MnSOD) and platelet endothelial cell adhesion molecule (PECAM) (markers of cardiomyocytes, mitochondria and the endothelium, respectively), revealed that MnSOD immunostaining overlapped that for α-actinin but not for PECAM (**Fig. 2f**). Taken together, the accumulation of fluorescent dyes that label mitochondria may reflect high mitochondria abundance in the heart.

Next, we treated dissociated cells obtained from E11.5 to E13.5 whole rat embryos with TMRM and analyzed them on a FACS (**Fig. 2g**). Some cells in this preparation were autofluorescent, which was due to the presence of lipopigments and flavins[13]. To obtain only TMRM-fluorescent cells and eliminate contamination by autofluorescent cells, we adopted pseudo-two-dimensional separation (**Fig. 2g** and Online Methods). We isolated populations with the highest TMRM-fluorescence from dispersed cells of E11.5, E12.5 and E13.5 whole rat embryos. The sorted cells from E11.5 embryos were immunostained for α-actinin (purity 99%, n = 3 embryos; yield, ~5 × 10^3 cells per embryo). We obtained similar results with E12.5 and E13.5 embryos. At these embryonic stages (E11.5–E13.5), the embryos contain skeletal myoblasts only and not mature myotubes. We found that mature skeletal myotubes, which could not pass through the FACS, could be marked with TMRM, whereas skeletal myoblasts, which do pass through the FACS, were not marked by TMRM (**Supplementary Fig. 6**).

Purification of PSC-derived cardiomyocytes

We first observed cardiomyocytes differentiated from mouse ESCs on day 7 of differentiation; the cells had marked TMRM accumulation. After TMRM staining, we fixed the cells and immunostained them for Nkx2.5 and α-actinin (**Fig. 3a**). The Nkx2.5– and α-actinin–positive areas and TMRM-positive area in the mouse

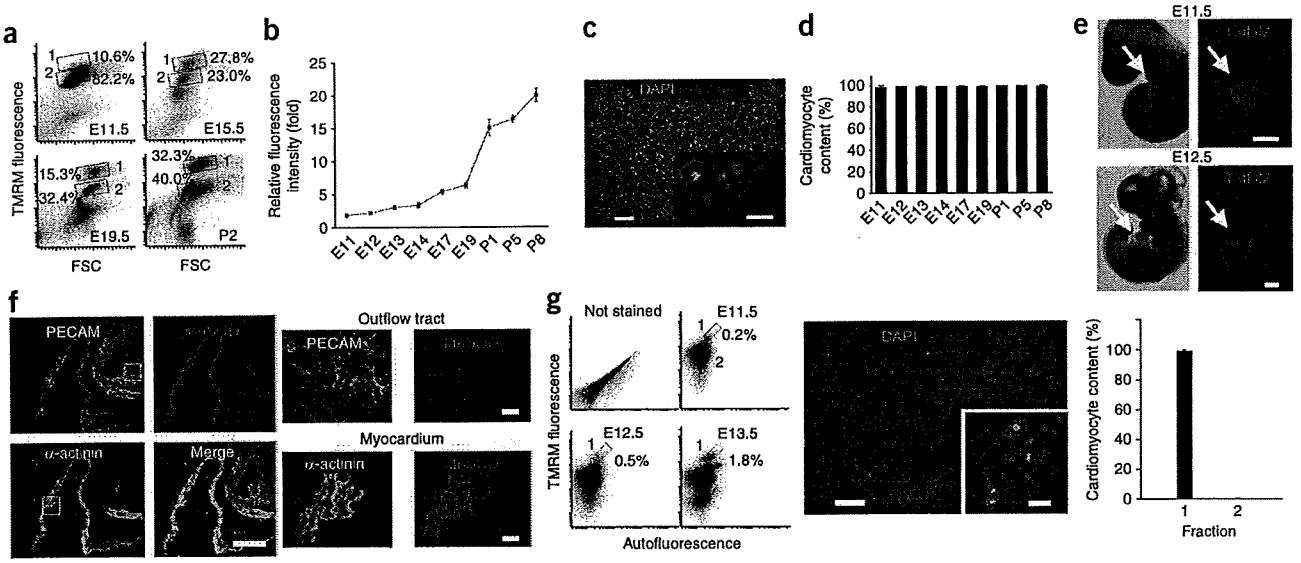

Figure 2 | Purification of cardiomyocytes from embryonic heart and whole embryo. (**a**) Representative FACS analysis of TMRM-stained rat embryonic heart cells at the indicated ages. Fractions 1 and 2 were typical gates for cardiomyocytes and noncardiomyocytes, respectively. (**b**) Relative fluorescence intensity of fraction 1 versus fraction 2 in the developing rat heart. Data are shown as mean ± s.d. (n = 3). (**c**) Immunofluorescence staining for α-actinin in the fraction 1 gated cells from E11.5 rat heart. (**d**) Cardiomyocyte content of the fraction 1-gated cells obtained from E11.5–P8 rat hearts. Data are shown as mean ± s.d. (n = 3). (**e**) Bright field (left) and fluorescence (right) images of whole rat embryos of indicated ages. (**f**) Immunofluorescence staining of rat E11.5 embryo for the indicated markers, PECAM, α-actinin and MnSOD. Images show pericardiac area (left four) and magnification of the boxed areas is shown on the right. (**g**) FACS analysis (left) of dissociated cells from whole embryos in the absence (not stained) or presence of TMRM at the indicated stages. Boxes indicate fractions 1 and 2; percentages of fraction 1 cells are shown. Immunofluorescence staining (middle) for α-actinin in the cells obtained from fraction 1 of E11.5 embryos. Cardiomyocyte content of fractions 1 and 2 at E11.5 is shown (right). Data are shown as mean ± s.d. (n = 3). Scale bars, 100 μm (**c**,**g**,**e**); 200 μm (**f** left); and 20 μm (**c** inset, **f** right, **g** inset).

ESC–derived cardiomyocytes were colocalized completely, although the intracellular localization of TMRM, Nkx2.5 and α-actinin was clearly different. Notably, TMRM dissociated rapidly into the bulk solution compared with other dyes upon fixation (**Supplementary Fig. 7**), indicating that there is likely to be no effect of TMRM on subsequent immunohistochemical analysis.

We applied pseudo–two-dimensional FACS analysis to the embryoid body–derived cells (**Fig. 3b**). We first observed fraction 1 cells 7 d after embryoid body formation. Both the ratio of the mean TMRM fluorescence in fraction 1 (cardiomyocytes) to fraction 2 (noncardiomyocytes) and the percentage of cells in fraction 1 increased gradually until day 15 (**Fig. 3c,d**), suggesting that the best time for obtaining mouse ESC–derived cardiomyocytes was at day 15.

We sorted approximately 5×10^5 to 9×10^5 cells from day 15 embryoid bodies. The viability of the sorted cells was 99.1 ± 1.5%, as confirmed by trypan blue staining (**Supplementary Fig. 8**). This high viability may be due to the fact that the cells were sorted based on TMRM accumulation (and thus contained active mitochondria). We cultured the sorted cells for 7 d to allow the cells to attach to the substrate and to elongate (Online Methods). Immunofluorescence staining for α-actinin and Nkx2.5 in three independent experiments confirmed that these cells were high-purity cardiomyocytes (99.5 ± 0.3%; **Fig. 3e**). We obtained >99% pure ESC-derived cardiomyocytes from day 12–25 embryoid bodies (**Fig. 3f**). We also obtained highly pure cardiomyocytes from mouse iPSCs (**Fig. 3g,h**).

To investigate the possibility of isolating cardiac progenitor cells, we stained whole E7.5 and E7.75 embryos. We found that TMRM faintly, but distinctly, marked the cardiac crescent, which contains cardiomyogenic precursor cells, indicating a possible applicability of our method to obtaining progenitor cells. Next, we carried out time-lapse fluorescence microscopy on attached mouse embryoid bodies stained with TMRM (**Supplementary Fig. 9**). We first observed TMRM-positive cells on day 6.5. Fluorescence in these cells increased gradually between days 6.5 and 7 and they started beating on day 7.0. In contrast, TMRM-negative cells did not beat during the experiments. We then performed FACS analysis on dissociated cells obtained from day 3–6.5 embryoid bodies and stained with TMRM. There were no cells in fraction 1. The higher TMRM-fluorescence cells in fraction 2 from day 3 and 4 embryoid bodies did not differentiate into cardiomyocytes, even after subsequent culture of attached cells for up to 8 d. In the case of day 6.5 embryoid bodies, some of the isolated cells differentiated into cardiomyocytes upon subsequent culture for 3 d. We also stained *Nkx2.5-GFP* knock-in mouse ESCs[6], which we and others have used frequently to isolate cardiomyocytes. After embryoid body formation, we first observed GFP fluorescence on day 7, whereas we observed TMRM staining on day 6.5 (**Supplementary Fig. 10**). Our observations indicate that our method can be used to purify differentiated cardiomyocytes but not cardiac progenitor cells.

We differentiated common marmoset ESCs, human ESCs and human iPSCs into cardiomyocyte-containing embryoid bodies by conventional floating cell culture. We transferred the embryoid bodies into the cell-attachment dishes with 10 nM TMRM. Beating embryoid bodies had extremely high TMRM fluorescence compared with that of nonbeating embryoid bodies derived from marmoset and human ESCs (**Fig. 4a**). Then we dispersed embryoid body–derived cells, stained them with TMRM and analyzed them on a FACS (**Fig. 4b**). We fixed sorted human

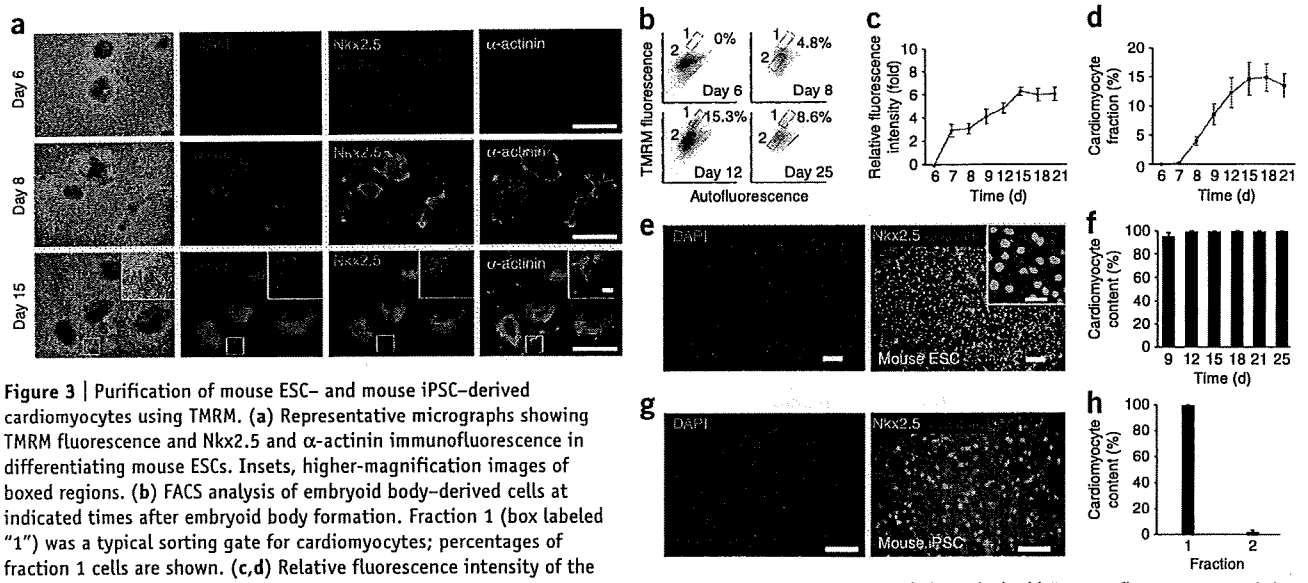

Figure 3 | Purification of mouse ESC- and mouse iPSC-derived cardiomyocytes using TMRM. (**a**) Representative micrographs showing TMRM fluorescence and Nkx2.5 and α-actinin immunofluorescence in differentiating mouse ESCs. Insets, higher-magnification images of boxed regions. (**b**) FACS analysis of embryoid body-derived cells at indicated times after embryoid body formation. Fraction 1 (box labeled "1") was a typical sorting gate for cardiomyocytes; percentages of fraction 1 cells are shown. (**c**,**d**) Relative fluorescence intensity of the fraction 1 versus fraction 2 cells (**c**) and percentage of cells in fraction 1 (**d**) over time. Data are mean ± s.d. ($n = 3$). (**e**–**h**) Immunofluorescence staining for Nkx2.5 and α-actinin in cultured fraction 1 cells sorted from day 15 embryoid bodies differentiated from mouse ESCs (**e**) and from mouse iPSCs (**g**); and cardiomyocyte content in cultured cells sorted from day 9–25 embryoid bodies differentiated from mouse ESCs (**f**) and in cultured cells sorted from day 15 embryoid bodies differentiated from mouse iPSCs (**h**). Data are mean ± s.d. ($n = 3$). Scale bars, 1 mm (**a**); and 100 μm (**a** inset, **e**,**g**).

cells in fraction 1, immunostained them for Nkx2.5 and subjected them to a second FACS analysis. The results showed that over 99.9% of cells in fraction 1 were cardiomyocytes (**Fig. 4c**). Furthermore, we compared expression of cardiac and noncardiac genes in human ESC–derived cardiomyocytes isolated by our method and in unpurified cells from embryoid bodies using real-time PCR. We observed a marked increase in the expression of myocardial genes and a decrease in the expression of nonmyocardial genes in purified human ESC–derived cardiomyocytes (**Supplementary Fig. 11**).

We also cultured the sorted cells for 5 d and immunostained them for Nkx2.5 and α-actinin (**Fig. 4d**). Common marmoset ESC, human ESC and human iPSC fraction 1 comprised 99.0 ± 1.0%, 99.0 ± 0.9% and 99.3 ± 0.2% cardiomyocytes, respectively; in contrast, fraction 2 had 2.3 ± 0.6%, 2.5 ± 0.2% and 1.7 ± 1.6% cardiomyocytes, respectively (**Fig. 4e**). To estimate the acquisition efficiency in the sorting experiments, we compared by FACS analysis the cardiomyocyte fraction obtained by TMRM with that obtained by immunofluorescence staining for α-actinin. The number of cardiomyocytes isolated by TMRM staining was 60–90% of the number defined by α-actinin staining (**Supplementary Fig. 12**). To rule out the possibility of skeletal muscle contamination in the sorted cardiomyocyte population, we extracted total mRNA from sorted cardiomyocytes and evaluated it for *myoD* expression using real-time PCR. We confirmed that there was no amplification of *myoD* (**Supplementary Fig. 13**).

No teratoma formation

We cultured the purified mouse ESC-derived cardiomyocytes and noncardiomyocytes for 7 d and found that although noncardiomyocytes formed piled-up colonies, in which some cells

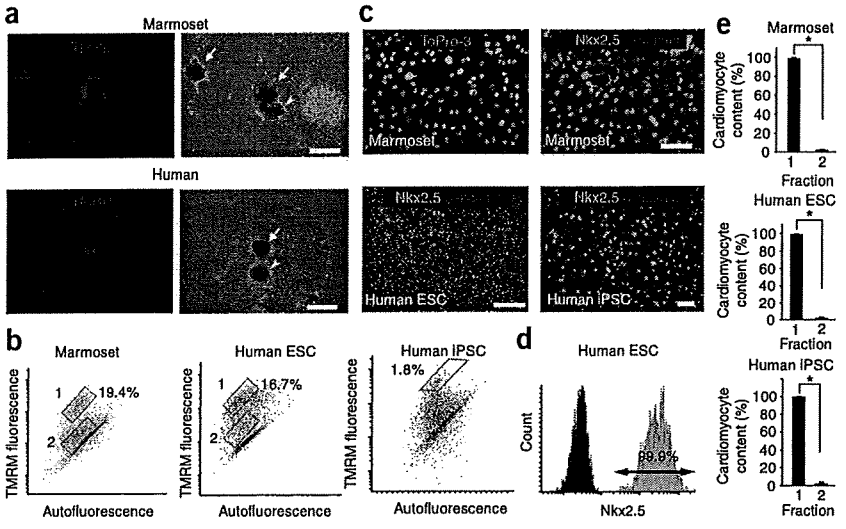

Figure 4 | Purification of PSC-derived cardiomyocytes in human and marmoset. (**a**) TMRM fluorescence (left) and phase contrast (right) images of marmoset and human embryoid bodies containing beating cardiomyocytes. Arrows, beating areas; arrowheads, nonbeating areas. (**b**) FACS separation of TMRM-stained cardiomyocytes derived from common marmoset ESCs, human ESCs and human iPSCs. Fractions 1 and 2 are boxed; percentages of fraction 1 cells are shown. (**c**) Immunofluorescence staining of fraction 1 cells for α-actinin and Nkx2.5. ToPro-3 represents nuclear staining. (**d**) Histogram showing immunodetection of Nkx2.5 (gray) and negative control (without first antibody; black) in sorted human ESC–derived fraction 1 cells. (**e**) The cardiomyocyte content of fractions 1 and 2 in common marmoset ESCs, human ESCs and human iPSCs. Data are mean ± s.d. ($n = 3$). *$P < 0.01$ (Student *t*-test). Scale bars, 500 μm (**a**); and 100 μm (**c**).

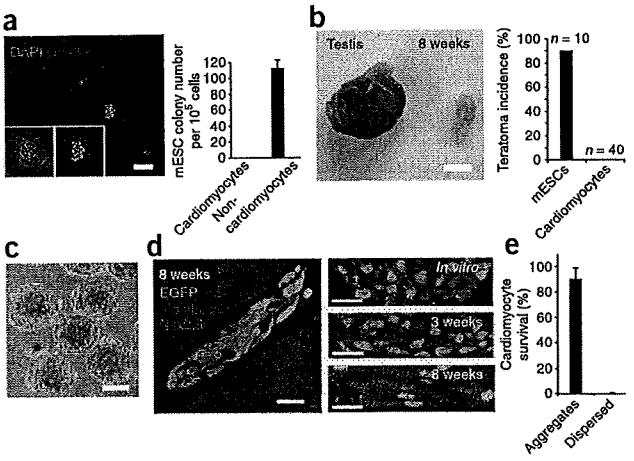

Figure 5 | Transplantation of purified mouse ESC-derived cardiomyocytes. **(a)** Immunofluorescence staining for Oct3/4 (red) in the sorted cells from the noncardiac fraction (left), and numbers of mouse ESC-like colonies obtained from 10^5 sorted cells (right). Data are mean ± s.d. ($n = 3$). **(b)** Transplantation of 250 undifferentiated mouse ESCs into testes resulted in teratoma formation (testis), whereas transplantation of 1.9×10^5 purified mouse ESC-derived cardiomyocytes did not (8 weeks). Incidence of teratoma formation was quantified (right). **(c)** Phase contrast image of mouse cardiomyocyte aggregates. **(d)** Immunofluorescence staining of engrafted mouse cardiomyocyte aggregates for α-actinin and Nkx2.5 8 weeks after transplantation (left); transplanted cells expressed EGFP. Mouse ESC-derived cardiomyocytes *in vitro* and 3 and 8 weeks after transplantation immunostained for Nkx2.5 and α-actinin (right). **(e)** Transplanted mouse ESC-derived cardiomyocyte survival. Data are shown as mean ± s.d. ($n = 5$). Scale bars, 100 μm (**a**,**c**); 5 mm (**b**); and 20 μm (**d**).

were positive for Oct3/4, the cardiomyocytes did not (**Fig. 5a**). Further, we transplanted 1.9×10^5 aggregated mouse ESC–derived cardiomyocytes and 250 undifferentiated mouse ESCs as a control into the testes of immunocompromised nonobese diabetic–severe combined immunodeficient (NOD-SCID) mice. Two months later, 90% of the control mice developed teratomas (9 of 10 mice), but we did not detect teratomas in any of the mice transplanted with purified mouse ESC–derived cardiomyocytes (0 of 40 mice) (**Fig. 5b**). We tried to verify that there was no teratoma formation in the heart by directly injecting mouse ESC–derived cardiomyocytes (1×10^5) into the myocardium of five NOD-SCID mice immediately after sorting. Two months later, we found few (<1%) of the transplanted cardiomyocytes in the heart (data not shown).

To understand the mechanism underlying this cell loss, we injected purified and MitoTracker Red–labeled neonatal rat cardiomyocytes into the left ventricular free wall of *ex vivo*–perfused hearts. We found one-third to one-half of injected cells in the postperfusion solution, indicating that the neonatal rat cardiomyocytes were washed out within the first 10 min (**Supplementary Fig. 14**). Next, we compared the tissue adhesiveness of purified mouse ESC–derived cardiomyocytes and mouse embryonic fibroblasts (MEFs) by counting cells in continuous sections of whole ventricles 24 h after injection into the left ventricular free walls. We found that less than 1% of the grafted ESC-derived cardiomyocytes had adhered to the host myocardium, compared with 50% of MEFs.

Transplantation of PSC-derived cardiomyocytes

From the above observations, we reasoned that loss of transplanted ESC-derived cardiomyocytes may be due to rapid washout and low adhesiveness of the cells. Because ESC-derived cardiomyocytes existed as homophilic cell aggregates (diameter, 100–500 μm) in mouse, marmoset and human embryoid bodies (**Supplementary Fig. 15**), we suspected that re-aggregated purified ESC-derived cardiomyocytes may be more resistant to rapid washout. We generated cardiomyocyte aggregates by seeding 313–10,000 purified mouse ESC–derived cardiomyocytes onto nonadhesive 96-well plates. One day after seeding, the cells adhered to each other, aggregated and started synchronized beating; 5 d later, cardiomyocyte aggregates formed with diameters of 100–450 μm (**Fig. 5c**, **Supplementary Fig. 16** and **Supplementary Video 2**). Propidium iodide staining revealed that a high proportion of re-aggregated mouse ESC–derived cardiomyocytes were viable (98.8 ± 0.2% of seeded cells; **Supplementary Fig. 16**).

We transplanted mouse cardiomyocyte aggregates into the ventricular free walls of NOD-SCID mice and killed the mice at 3 and 8 weeks ($n = 5$ for both groups). We observed no teratoma formation in either group. Immunofluorescence staining revealed that cell aggregates positive for the tracers Nkx2.5 and α-actinin were located in the left ventricle (**Fig. 5d**). The number of cells that survived in the heart was greater than 90% (**Fig. 5e**). Furthermore, we repeated these experimental procedures using purified human ESC–derived cardiomyocytes (**Supplementary Video 3**). Two months after transplantation, we detected a large amount of human myocardial tissue in NOD-SCID mouse heart (**Supplementary Fig. 17**).

Finally, we investigated which autoparacrine factors are important for the survival of ESC-derived cardiomyocytes. Human cardiomyocyte aggregates remained viable under serum-free culture conditions; moreover, their diameters increased by approximately twofold by day 25. Supplementation of the cultures with physiological concentrations of basic fibroblast growth factor (bFGF), epidermal growth factor (EGF), platelet-derived growth factor beta dimer (PDGF-BB) and endothelin-1 (ET-1) strongly enhanced the growth of the cardiomyocyte aggregates (**Supplementary Fig. 18a** and **Supplementary Video 4**). We confirmed expression of these growth factors and their receptors by real-time PCR (probe and primer sets are listed in **Supplementary Table 1**). We also confirmed that these growth factors were expressed in adult human and mouse hearts (**Supplementary Fig. 18b**). Autoparacrine stimulation with these growth factors may be one reason why grafted cardiomyocyte aggregates survived and grew in the host myocardium.

DISCUSSION

Our method for cardiomyocyte isolation has two advantages. First, it does not require genetic modification of the cells. Genetic modifications using nonviral or viral systems have several disadvantages: extrinsic genes may be silenced, the number of integration events in one cell is difficult to control, targeted integration is not straightforward, and line selection as well as verification of proper expression of extrinsic genes[14] is time-consuming. Furthermore, genetic modification carries risks such as possible tumor formation[15–17]. Second, our method is likely to be widely applicable. We demonstrated that it may be used to purify ESC-derived cardiomyocytes in four species, including human,

and that it is also applicable to mouse and human iPSCs. High abundance of cellular mitochondria is likely to be a common characteristic of cardiomyocytes irrespective of species. In contrast, most genetic modifications require species-specific constructs. Our simple purification strategy should facilitate basic studies using embryonic heart and stem cell–derived cardiomyocytes; furthermore, this strategy can also allow isolation of noncardiomyocytes, which may open up new approaches to studying developmental interactions.

The ESC-derived cardiomyocytes purified using our method did not induce teratoma formation in either the heart or testes. Although from the viewpoint of clinical safety, further studies using large animal models with a much larger number of ESC-derived cardiomyocytes will be required, we believe that our purification method may have considerable advantages over existing methods for eventual clinical translation as well.

Our results suggest that induction of mitochondrial biogenesis begins shortly before beating of cardiomyocytes. This indicates the tight relationship between cardiomyogenesis and mitochondrial biogenesis. A combination of our strategy and other marking techniques for cardiac progenitor cells may facilitate study in this field.

Unpurified fetal and neonatal rat cardiomyocytes and bone marrow mesenchymal and ESC-derived cardiomyocytes have been shown to survive in the recipient heart[18–20]. In contrast, purified and dispersed cardiomyocytes differentiated from ESCs did not achieve a high survival rate[5]. Re-aggregation augmented the long-term survival of purified mouse and human ESC–derived cardiomyocytes. Our results indicate that ESC-derived cardiomyocytes might be highly anchorage-dependent, and that homophilic cell-to-cell adhesion and autoparacrine signaling may be important factors contributing to their survival.

METHODS

Methods and any associated references are available in the online version of the paper at http://www.nature.com/naturemethods/.

Note: Supplementary information is available on the Nature Methods website.

ACKNOWLEDGMENTS

Human ESCs were a gift of N. Nakatsuji at the Department of Development and Differentiation, Institute for Frontier Medical Sciences, Kyoto University. Human and mouse iPSCs were a gift of S. Yamanaka at the Center for iPS Cell Research and Application, Institute for Integrated Cell-Material Sciences, Kyoto University. Mouse ESCs were a gift of H. Niwa at the Laboratory of Pluripotent Cell Studies, RIKEN Center for Developmental Biology. This study was supported in part by research grants from the Ministry of Education, Science and Culture, Japan, and by the Program for Promotion of Fundamental Studies in Health Science of the National Institute of Biomedical Innovation.

AUTHOR CONTRIBUTIONS

F.H. designed the whole study. F.H. performed most experiments and wrote the manuscript. H.C. participated in cell-sorting experiments and prepared cells. H.Yamashita participated in cell-sorting experiments, PCR experiments, immunofluorescent staining, animal experiments and preparing cells. S.T., Y.S., W.L., T.T., T.O., K.S., Y.O. and T.E. participated in cell preparations. H.Yamakawa and M.M. participated in heart perfusion experiments. K.H. and T.M. provided the *Nkx2.5 knock-in* ESCs. S.Y., M.M., R.K., M.S., S.M. and S.O. provided advice. E.S. provided cmESCs. T.S. supervised Y.S. K.F. provided advice, obtained the budget and supervised the project.

COMPETING INTERESTS STATEMENT

The authors declare competing financial interests: details accompany the full-text HTML version of the paper at http://www.nature.com/naturemethods/.

Published online at http://www.nature.com/naturemethods/.
Reprints and permissions information is available online at http://npg.nature.com/reprintsandpermissions/.

1. Yuasa, S. *et al.* Transient inhibition of BMP signaling by Noggin induces cardiomyocyte differentiation of mouse embryonic stem cells. *Nat. Biotechnol.* **23**, 607–611 (2005).
2. Nemir, M., Croquelois, A., Pedrazzini, T. & Radtke, F. Induction of cardiogenesis in embryonic stem cells via downregulation of Notch1 signaling. *Circ. Res.* **98**, 1471–1478 (2006).
3. Mummery, C. *et al.* Differentiation of human embryonic stem cells to cardiomyocytes: role of coculture with visceral endoderm-like cells. *Circulation* **107**, 2733–2740 (2003).
4. Anderson, D. *et al.* Transgenic enrichment of cardiomyocytes from human embryonic stem cells. *Mol. Ther.* **15**, 2027–2036 (2007).
5. Kolossov, E. *et al.* Engraftment of engineered ES cell-derived cardiomyocytes but not BM cells restores contractile function to the infarcted myocardium. *J. Exp. Med.* **203**, 2315–2327 (2006).
6. Hidaka, K. *et al.* Chamber-specific differentiation of Nkx2.5-positive cardiac precursor cells from murine embryonic stem cells. *FASEB J.* **17**, 740–742 (2003).
7. Fijnvandraat, A.C. *et al.* Cardiomyocytes purified from differentiated embryonic stem cells exhibit characteristics of early chamber myocardium. *J. Mol. Cell. Cardiol.* **35**, 1461–1472 (2003).
8. Gassanov, N., Er, F., Zagidullin, N. & Hoppe, U.C. Endothelin induces differentiation of ANP-EGFP expressing embryonic stem cells towards a pacemaker phenotype. *FASEB J.* **18**, 1710–1712 (2004).
9. Huber, I. *et al.* Identification and selection of cardiomyocytes during human embryonic stem cell differentiation. *FASEB J.* **21**, 2551–2563 (2007).
10. Klug, M.G., Soonpaa, M.H., Koh, G.Y. & Field, L.J. Genetically selected cardiomyocytes from differentiating embronic stem cells form stable intracardiac grafts. *J. Clin. Invest.* **98**, 216–224 (1996).
11. Laflamme, M.A. *et al.* Cardiomyocytes derived from human embryonic stem cells in pro-survival factors enhance function of infarcted rat hearts. *Nat. Biotechnol.* **25**, 1015–1024 (2007).
12. Xu, C., Police, S., Hassanipour, M. & Gold, J.D. Cardiac bodies: a novel culture method for enrichment of cardiomyocytes derived from human embryonic stem cells. *Stem Cells Dev.* **15**, 631–639 (2006).
13. Monici, M. Cell and tissue autofluorescence research and diagnostic applications. *Biotechnol. Annu. Rev.* **11**, 227–256 (2005).
14. Gropp, M. & Reubinoff, B. Lentiviral vector-mediated gene delivery into human embryonic stem cells. *Methods Enzymol.* **420**, 64–81 (2006).
15. Tsukahara, T. *et al.* Murine leukemia virus vector integration favors promoter regions and regional hot spots in a human T-cell line. *Biochem. Biophys. Res. Commun.* **345**, 1099–1107 (2006).
16. Recchia, A. *et al.* Retroviral vector integration deregulates gene expression but has no consequence on the biology and function of transplanted T cells. *Proc. Natl. Acad. Sci. USA* **103**, 1457–1462 (2006).
17. Woods, N.B. *et al.* Lentiviral vector transduction of NOD/SCID repopulating cells results in multiple vector integrations per transduced cell: risk of insertional mutagenesis. *Blood* **101**, 1284–1289 (2003).
18. van Laake, L.W. *et al.* Human embryonic stem cell-derived cardiomyocytes survive and mature in the mouse heart and transiently improve function after myocardial infarction. *Stem Cell Rev.* **1**, 9–24 (2007).
19. Reinecke, H., Zhang, M., Bartosek, T. & Murry, C.E. Survival, integration, and differentiation of cardiomyocyte grafts: a study in normal and injured rat hearts. *Circulation* **100**, 193–202 (1999).
20. Hattan, N. *et al.* Purified cardiomyocytes from bone marrow mesenchymal stem cells produce stable intracardiac grafts in mice. *Cardiovasc. Res.* **65**, 334–344 (2005).

ONLINE METHODS

Mouse, common marmoset and human PSCs. Mouse ESCs were obtained from Laboratory of Pluripotent Cell Studies, RIKEN Center for Developmental Biology. Common marmoset ESCs (cmESCs) were obtained from Central Institute for Experimental Animals. The human ESC lines (khESC-1, 2 and 3) were obtained from Department of Development and Differentiation, Institute for Frontier Medical Sciences, Kyoto University and were used in conformity with The Guidelines for Derivation and Utilization of Human Embryonic Stem Cells of the Ministry of Education, Culture, Sports, Science and Technology, Japan. Mouse (iPS-MEF-Ng-20D-17) and human (253G4) iPSCs were obtained from Center for iPSC Research and Application, Kyoto University.

Animals. All animals including pregnant and neonatal Wistar rats, and NOD-SCID mice (10 weeks old, male), were purchased from Japan CLEA.

All experimental procedures and protocols were approved by the Animal Care and Use Committees of the Keio University and conformed to the US National Institutes of Health Guide for the Care and Use of Laboratory Animals.

Reagents. MitoTracker dyes (Deep Red, Red, Orange and Green), TMRM, 5,5′,6,6′-tetrachloro-1,1′,3,3′-tetraethylbenzimidazolylcarbocyanine iodide (JC-1), nonyl acridine orange (NAO) and Rhodamine 123 were purchased from Invitrogen. These mitochondria-selective fluorescent dyes can be divided into the Nernstian or non-Nernstian dye groups. The former, including TMRM, can enter into and exit from the mitochondrial matrix freely depending on the mitochondrial membrane potential. In contrast, non-Nernstian dyes such as the MitoTracker dyes cannot exit freely[21]. This characteristic difference may reflect their toxicities and can be used case by case for research, for example, non-Nernstian dyes are used for long-term staining.

The mouse monoclonal antibody to α-actinin (used at 1:400 dilution) was purchased from Sigma-Aldrich. The goat polyclonal antibody to GATA-4 (C-20) and the goat polyclonal antibody for Nkx2.5 (N-19) were purchased from Santa Cruz biotechnology. The mouse monoclonal antibody for SdhB (1:100), Alexa Fluor 488 donkey anti-mouse IgG antibody and Alexa Fluor 546 donkey anti-goat immunoglobulin gamma (IgG) were purchased from Invitrogen.

Maintenance of mouse, marmoset and human PSCs. We maintained mouse ESCs and iPSCs on gelatin-coated dishes in Glasgow Minimum Essential Medium (Sigma) supplemented with 10% FBS (FBS; Equitechbio), 0.1 mM MEM Non-Essential Amino Acids solution (Sigma), 2 mM L-glutamine (Sigma), 0.1 mM β-mercaptoethanol (Sigma) and 2,000 U ml^{-1} mouse LIF (Chemicon). We maintained cmESCs on mouse embryonic fibroblasts in Knockout Dulbecco's Modified Eagle's Medium (KO-DMEM; Invitrogen) supplemented with 20% Knockout Serum Replacement (KSR; Invitrogen), 0.1 mM MEM Non-Essential Amino Acids solution, 2 mM L-glutamine, 0.1 mM β-mercaptoethanol and 4 ng ml^{-1} basic fibroblast growth factor (bFGF; Wako Pure Chemical). We maintained human ESCs and iPSCs similarly to cmESCs, except that Dulbecco's Modified Eagle's Medium/Nutrient Mixture F-12 Ham 1:1 (DMEM-F12; Sigma) was used instead of KO-DMEM.

Differentiation of mouse PSC–derived cardiomyocytes. We performed *in vitro* differentiation of mouse ESCs and iPSCs as described below. We collected mouse PSCs with 0.25% trypsin-EDTA and dissociated them. Seventy-five cells were formed to one embryoid body in one hanging drop with alpha-modified Eagle medium (αMEM; Sigma) supplemented with 10% FBS (Equitechbio). On day 2, we transferred embryoid bodies into floating culture plate with new medium. Four to five days after differentiation, floating embryoid bodies were transferred into attachment culture with nonserum culture medium: αMEM supplemented with insulin-transferrin-selenium (ITS; Sigma). Typically, beating cells appeared on day 7. Embryoid bodies were used for purification experiments between days 12 and 25.

Differentiation of cmESC–derived cardiomyocytes. We performed differentiation of cmESCs as follows. The colonies were detached with 0.1% type three collagenase (Worthington Biochemical) and cultured in cmESC medium lacking bFGF or αMEM and supplemented with 10% FBS (SAFC Biosciences) and 0.1 mM β-mercaptoethanol in bacterial Petri dishes to form embryoid bodies. Typically, 5–20% of embryoid bodies contained beating cells. Embryoid bodies were washed three times with αMEM between days 18 and 25, and cultured with αMEM supplemented with ITS. Embryoid bodies were used for purification experiments between days 30 and 50.

Differentiation of human PSC–derived cardiomyocytes. We grew the detached undifferentiated colonies of human ESCs and iPSCs with αMEM supplemented with 20% FBS (SAFC Biosciences) and 0.1 mM β-mercaptoethanol in bacterial Petri dishes to form embryoid bodies. We observed embryoid bodies containing rhythmically beating cells 16–20 d later. Typically, 1–5% of embryoid bodies contained beating cells. From days 20 to 40, embryoid bodies were washed three times with αMEM and cultured with αMEM supplemented with ITS. Embryoid bodies were used for purification experiments between days 50 and 90.

Staining of cultured embryos. We isolated E11.5 and E12.5 Wistar rat embryos and stained with 50 nM TMRM for 4 h in DMEM with 20% FBS at 30% O_2, 5% CO_2 and 37 °C. Then, we changed to medium without TMRM and incubated the embryos for 4 h to remove unbound dye. We observed the fluorescence signal using conventional fluorescence laser microscopy (IX70 microscope (Olympus) equipped with a color charge-coupled device (CCD) camera (CS220; Olympus)).

Staining *in vivo* embryos. We carried out abdominal surgery on the pregnant Wistar rat on postcoital day 11 under deep anesthesia. We carried out a shallow injection of 100 μl of 500 nM MitoTracker Red solution into the placental side of the exposed ovaries. The rat was sustained under anesthesia for 6 h. Then, under deep anesthesia, we removed the embryos from the rat and observed them using fluorescence microscopy. About 20% of the embryos were positive for MitoTracker Red.

Cardiomyocyte purification. We dispersed the minced hearts, whole rat embryos, or intact embryoid bodies using 0.1% collagenase (Worthington Biochemical), 0.25% trypsin (Becton Dickinson), 20 μg ml^{-1} DNase I (Sigma) and the appropriate

concentration of dyes (10 nM TMRM, 50 nM NAO, 1.5 μM JC-1 or 50 nM MitoTrackers) in Ads buffer (116 mM NaCl, 20 mM HEPES, 12.5 mM NaH_2PO_4, 5.6 mM glucose, 5.4 mM KCl and 0.8 mM $MgSO_4$; pH 7.35) with stirring for 30 min. The dispersed cells were collected and residual cell aggregates were digested again with the same digestion medium. We continued this procedure until all cells were completely dissociated. Finally, all dispersed cells were dissociated with Ads buffer and then analyzed on a FACS (FACS Aria; Becton Dickinson) using 515–545 and 556–601 nm bandpass filters to detect green and red, respectively.

In many cases, nonstained cells exhibited autofluorescence, which may be due to the presence of lipopigments and flavins having broad emission spectrum (450–650 nm)[13]. We suspected that this may affect purity of cardiomyocytes. TMRM can be excited by a 488-nm semiconductor laser and has an emission spectrum that coincides with the red bandpass filter (peak at 575 nm and only 10% of peak fluorescence at 545 nm). Thus, to obtain only cells with high TMRM fluorescence and eliminate contaminating autofluorescent cells, we adopted 'pseudo–two-dimensional separation' in which we observed cells both with red and green filters. In other words, cardiomyocytes received 488 excitation, and then selection for low green and high red fluorescence. Pregating for eliminating doublet fractions, in which one droplet contains more than two cells, was performed according to the manufacturer's instructions.

The TMRM-labeled sorted cells were collected into a tube or were seeded into culture dishes with αMEM containing 10% FBS. For sequential estimation of cardiomyocyte purity, we fixed the sorted cells immediately after collection, then stained them with Nkx2.5 antibody and analyzed again on a FACS. For culture, we used a plate equipped with flexiPERM conA (Greiner Bio-One GmbH) following the manufacturer's instructions. The flexiPERM vessel is a reusable culture funnel, which can adhere tightly onto plastic and glass surfaces. One day after sorting, the flexiPERM vessel was detached from the culture plate and the appropriate amount of medium was added to the plate. This system allowed high-density culture of purified cardiomyocytes in the center of the dish, which enabled good microscopic observation of all cells after detachment of the vessel. For all PSCs, seeded cells were cultured for 5–7 d with αMEM containing 10% FBS, which is necessary for the cells to attach, elongate and develop sarcomere structure, and then fixed and immunofluorescence-stained for α-actinin and Nkx2.5. The culture step is not required for achieving high-purity cardiomyocyte isolation because we have more directly estimated cardiomyocyte purity by sequential FACS analysis.

Transplantation. We purified mouse and human ESC–derived cardiomyocytes, distributed them into nonadhesive 96-well plates (Sumitomo Bakelite) and centrifuged them for 5 min at 100*g*. Two weeks later, the aggregates formed were stained with 50 μM of MitoTracker Red for 2 h in the incubator and washed extensively with Ads buffer. After lightly anesthetizing seven-week-old male NOD-SCID mice with diethylether (Wako Pure Chemical), we intubated them under anesthetization with 1.5% forane (isoflurane, 2-chloro-2-(difluoromethoxy)-1,1,1-trifluoro-ethane) and mechanically ventilated with a Harvard respirator. After this, we performed a left thoracotomy at the third intercostal space and exposed the heart. We inserted a small dead-volume syringe equipped with a 30G needle (Becton Dickinson) containing reaggregated purified cardiomyocytes into the apex, proximally advanced 2–3 mm into the myocardium and released the cells into the myocardium. Then we closed the chest and maintained the mice for 8 weeks before performing a histological examination of these mice.

The 3-(4,5-dimethyl-thiazol-2-yl)-2,5-diphenyltetrazolium bromide (MTT) assay. We treated primary neonatal rat cardiomyocytes with various mitochondrial indicators at 50 nM and 100 nM for 24 h. We added MTT (Wako Pure Chemical) at 0.5 mg ml^{-1} and incubated the cardiomyocytes for 3 h. Then, we dissolved the formazan salt that formed in dimethyl sulfoxide. The absorbance was measured at a wavelength of 550 nm with the background subtracted at 690 nm (SmartSpec3000; Bio-Rad Laboratories). Data were presented as percentage of formazan formation compared to control cells.

Immunofluorescence staining. We fixed cells with 4% paraformaldehyde in phosphate-buffered saline (PBS; pH 7.0) for 20 min. Subsequently, cells were permeabilized with 0.2% Triton X-100 (Sigma) at room temperature (20–28 °C) for 10 min, and then incubated with the primary antibody at 4 °C overnight. Cells were washed with TBS containing 0.1% Tween-20 four times before incubation with the secondary antibodies at room temperature for 30 min. After nuclear staining with DAPI or ToPro-3 (Invitrogen), fluorescence signals were observed using fluorescence microscopy (IX71; Olympus) or confocal laser microscopy (LSM510 META; Carl Zeiss), respectively.

For tissue samples, mice were killed using pentobarbital. The hearts were then perfused from the apex with PBS and fixed by perfusion with 4% paraformaldehyde in PBS (Muto Pure Chemicals). The hearts were then dissected, cryoprotected in sucrose at 4 °C overnight, embedded in OCT compound (Sakura Finetec) and snap-frozen in liquid nitrogen.

Re-aggregation of purified human ESC–derived cardiomyocytes and long-term culture without serum. Human ESC–derived cardiomyocytes were purified and suspended in αMEM supplemented with insulin, transferrin and selenium (ITS) and 0.05% BSA (Invitrogen) in the absence or presence of one of the following growth factors: 25 ng ml^{-1} bFGF (Wako Pure Chemicals); 25 ng ml^{-1} acidic FGF (aFGF); 25 ng ml^{-1} FGF-4; 20 ng ml^{-1} keratinocyte growth factor (KGF); 100 ng ml^{-1} stem cell factor (SCF); 100 ng ml^{-1} vascular endothelial growth factor (VEGF); 10 ng ml^{-1} LIF (Chemicon); 100 ng ml^{-1} glial cell line–derived neurotrophic factor (GDNF); 20 ng ml^{-1} hepatocyte growth factor (HGF); 10 ng ml^{-1} insulin-like growth factor (IGF)-1; 100 ng ml^{-1} epidermal growth factor (EGF); 1×10^{7} M endothelin-1 (ET-1); 10 ng ml^{-1} platelet-derived growth factor (PDGF)-AA; and 100 ng ml^{-1} PDGF-BB. Unless indicated otherwise, growth factors were purchased from R&D Systems Inc. Five hundred cells were distributed into each well ($n = 8$) of cell nonadhesive 96-well plates (MS-0096S; Sumitomo Bakelite) and centrifuged for 5 min at 100*g*.

Total RNA extraction, cDNA synthesis and real-time PCR. Total RNA was prepared from tissues and embryoid bodies using ISOGEN (Nippon gene), according to the manufacturer's instructions. Contaminating genomic DNA was degraded by RNase-free DNase I

doi:10.1038/nmeth.1403